Università degli Studi di Milano

FACOLTÀ DI SCIENZE E TECNOLOGIE
Corso di Laurea Magistrale in Fisica

Anomalous diffusion of fluctuating Cooper pairs in superconducting films

Candidato:
Pietro Brighi
Matricola 883492

Relatori:
Prof. Luca Guido Arthur Molinari
Prof. Marco Grilli
Prof. Sergio Caprara

Anno Accademico 2016-2017

Contents

Introduction

Since its discovery in 1911 by Kammerling-Onnes ([5]), superconductivity has always been an intriguing topic in condensed matter physics. Many efforts have been spent by theorists through the years, in order to find an adequate solution explaining the microscopical mechanisms ruling the superconducting phase.

In 1935, Fritz and Heinz London attempted to explain superconductivity through a phenomenological model based on the idea of a an irrotational fluid of electrons in these materials [6]. The application of fluidodynamics laws then led to the first explanation of the Meissner-Ochesnfeld effect [7].

A few years later, a great success was achieved by Lev D. Landau and Vitaly Ginzburg [8] who applied their phenomenological theory of phase transitions [9] to superconductivity; this lead to the understanding of the behaviour of many physical quantities near the transition and, after a work by Abrikosov [10], to the description of the differences between type-I and type-II superconductors.

Despite the great successes achieved with the phenomenological approach, a microscopical theory was necessary, in order to understand the very nature of superconductors. This microscopical theory was indeed developed during the fifties by John Bardeen, Leon Cooper and Robert Schrieffer [14]. They suggested that in some materials, at low temperature, there exists an attractive interaction between electrons, mediated by the quanta of lattice vibrations: the phonons. This attraction leads to a bound state of two electrons, called Cooper pair, that thus create an energy gap Δ in the electronic spectrum in a very narrow range of energies in the proximity of E_F. The creation of pairs in these materials gives to electrons an order parameter, the phase of the wavefunction, resulting in the absence of resistivity.

This intuition revealed to be correct, as soon as comparison between theoretical predictions and experimental data showed a surpisingly great accord.

In spite of their exceptional agreement with observed phenomena, both Ginzburg-Landau and BCS theories are developed in a Mean Field Approximation (MFA). It is common, in physics, to use this approximation in order to work out otherwise unsolvable problems; in the great majority of cases, this approach can give qualitative insight, but fails when things get quantitative. This is because, in most systems, the effects beyond the MFA, known as fluctuations, have a significant role.

As shown by Ginzburg [19], this is not the case for bulk, type-I superconductors, where fluctuations show to become considerable only in a very narrow range of temperatures around T_c.

Nevertheless, through years, many particular superconductive materials have been discovered, whose behaviour MFA cannot account for. Even if Anderson proved ([53]) that disorder should not affect three-dimensional superconduc-

tors, when lower dimensionalities are taken into account this is not the case anymore. In these materials, impurity concentration plays a fundamental role, and fluctutations show to have a much larger action.

Many new techniques, both phenomenological and microscopical, have been created and are still used nowadays in order to account for these effects.

After Anderson's paper [33], the interplay between disorder-induced localization and charge transport became a hotly debated topic. In the eighties, Altshuler and Aronov started the investigation on the combination of Anderson's localization and of electron-electron interactions [27].

The developement of this subject opened the possibility of the occurrence of a transition from the superconducting phase to an insulator (SIT). The SIT was first introduced in the late eighties/early nineties and it is still nowadays an open subject.

About the Superconductor-Insulator Transition, many scientists proposed their own idea of the mechanism driving the passage from the two farthest scenarios in charge transport. Among them, two main frameworks arise: the fermionic and the bosonic hypothesis.

According to the first [48], Cooper pairs break up at the transition due to fluctuations in the amplitude of the order parameter, thus the superconducting phase disappears, leaving bare electrons that can localize as a consequence of disorder. The second one [31], on the contrary, suggests that Cooper pairs survive the transition, but phase fluctutations destroy their coherence hence they persist as localized bosons and therefore conductivity is zero.

At the present stage, none of this scenarios seems to be clearly the right one, since many experimental data have been found in agreement with predictions made by both of them. Nevertheless it seems that homogeneously disordered systems are ruled by fermionic transition, while granular films show a much more bosonic behaviour.

Some recent experiments [2] showed uncommon features in nominally homogeneous ultrathin NbN films. Characteristics belonging to the different schemes manifest on the same samples, suggesting that possibly a continuous evolutions between the two there may exist.

Novel features, such as a cross-over between a $2\mathcal{D}$ and a $0\mathcal{D}$-like paraconductivity trend, rose many questions on the fluctuations' behaviour in these films. The hypothesis of an anomalous diffusion of fluctuating Cooper pairs was proposed as a possible answer. In the same paper, it has been proved that this anomaly could indeed explain the behaviour in the excess conductivity.

We argue that in these niobium nitride thin films, a different type of disorder arises. Even if morphologically the samples seem to be homogeneously disordered, the electronic spectra showed that some other type of inhomogeneity is somehow present in the films. There are some regions where the pseudogap (i.e. the depression of the DOS around the Fermi energy above the critical temperature) is higher than the expected value. We call these areas *supergrains* and hypothesize that the anomalous diffusion law is strongly related to their presence.

The aim of this thesis is thus to calculate the DOS of this system, taking into account the anomalous diffusion in the fluctuations' propagator. We want to prove that this different type of disorder is effective in increasing the pseudogap and that the size of the supergrains obtained via our calculations matches the value obtained thorugh experiments.

The importance of this work relies in the novelty of the approach to fluctuations and to the interesting fact that the samples studied seem to belong to an intermediate region of disorder, where both the fermionic and the bosonic behaviours contribute. We hope, with this thesis, to obtain a comparison of the theoretical curves with tunneling spectra, in order to better understand the physics beyond this strange features. Certainly, more experimental effort in this sense should follow, as the results available at the moment are not enough to allow neither fitting nor statistical analysis.

Clearly, to get the real comprehension of the physical nature of this characteristics, a microscopic approach should be combined with this phenomenological study.

Finally, the structure of the following work is given: in chapter one the phenomenology of disordered and low-dimensional superconductors is presented, together with the two main theoretical frameworks of the SIT. Furthermore, we show in some detail the experimental data coming from [2] on NbN ultrathin films. In chapter two, we deal with the theoretical background on fluctuations explaining the main features characterising the disordered superconductor. In chapters three and four the results obtained with the anomalous diffusion law are presented and commented, highlighting their successes and their limits and suggesting further analysis in order to improve our understanding of these samples.

Chapter 1

Fluctuation phenomenology

Both the phenomenological theory of Ginzburg and Landau [8] (GL) and the quantum microscopical one of Bardeen, Cooper and Schriffer [14] (BCS), are developed in a Mean Field Approximation (MFA) framework. Although usually MFA gives only qualitative explanations, in the lucky case of superconductors, quantitative results are found in perfect agreement with experimental data of bulk, clean, type-I superconductors. This is because, as shown by Ginzburg [19], fluctuational effects, in these systems, are practically negligible. He calculated the fluctuations' contribution to heat capacity, finding that their effects are important in a very narrow range of temperatures $\delta T/T_c \sim 10^{-12} \div 10^{-14}$ K from the transition, so that this phenomenon is not experimentally accesible in bulk superconductors. Nevertheless, in the second half of the 20th century, after the discovery of dirty [47] and low dimensional [45],[46] superconductors, many new features came out, which MFA is not able account for. Generally speaking, fluctuations make the transition from the superconducting to the normal phase less sharp, often giving some *precursor* effects, at temperature $T \geq T_c$. Furthermore, thinness and disorder cause the transition temperature to decrease. In this chapter, we will briefly review the most important of these features, which gave rise to the need of analizing fluctuations in superconductors.

1.1 Experimental observations

In this section, we will present some of the most relevant phenomena connected to fluctuations, giving experimental evidence of their important role in some particular materials.

Moving away from the ideally clean, 3D, type-I superconductor, for which the BCS mean field approximation is in perfect agreement with experimental results, the situation becomes more complicated by all means. Even though deep inside the superconducting phase, the main characteristic, both electronical and termodynamical, of the material are not affected by fluctuational effects, both near and above the transition, these can change the behaviour of the sample.

The enhanced effect of fluctuations can be attributed to different physical reasons. Among them certainly disorder plays an important role, as well as dimensionality.

At a first glance the main effect of these is the decreasing of the critical

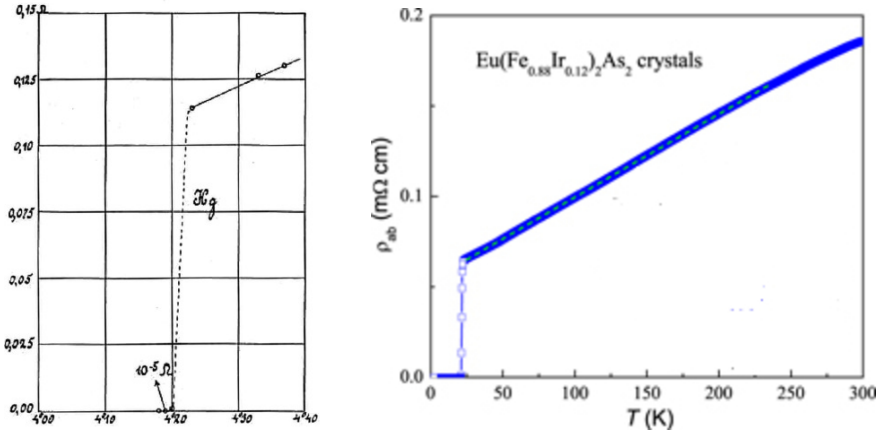

(a) *R vs T from the original work of Kamerling-Onnhes on Hg*

(b) *In plane resistivity (ρ_{ab}) vs T for $Eu(Fe_{0.88}Ir_{0.12})_2As_2$ sample ([59])*

Figure 1.1: *Resistance measurements in two different superconductors, the sharp transition at the critical temperature is well displayed in both cases.*

temperature and even its vanishing at a critical disorder concentration or thickness. The experimental results shown in fig.1.2, from [49], show an interesting behaviour of the transition temperature with the decrease of the film thickness t. For $t > 30$Å, the thinner the sample, the higher the transition temperature. Nevertheless, as soon as the thickness becomes smaller than this value, the samples show a dramatic decrease in T_c, thus establishing a difference between thin and ultrathin films. On the right panel the diagram for the sheet resistance as a function of thickness is displayed. Again at the same thickness value of $t \approx 30$Åthe the behaviour drastically changes and a huge increase in sheet resistance is observed for $t < 30$Å.

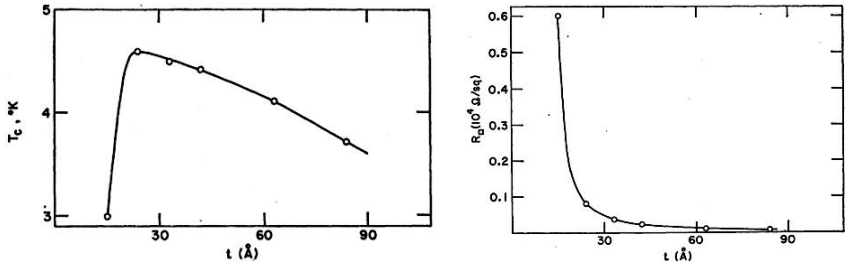

Figure 1.2: *T_c (left) and $R_\square$ (right) vs t (film thickness) for Al thin layers deposited on SiO substrates. We can observe how, at thickness $t < 30$Åthe critical temperature dramatically decreases while the sheet resistance has a huge increase.*

Furthermore, many other physical quantities show unexpected behaviours in these kind of superconductors, strongly deviating from their Mean Field Theory (MFT) values. These effects arise either in the smoothening of the transition or in precursor effects.

Among the firsts, certainly we can consider the resistance behaviour and the heat capacity jump for disordered and low-dimensional superconductors.

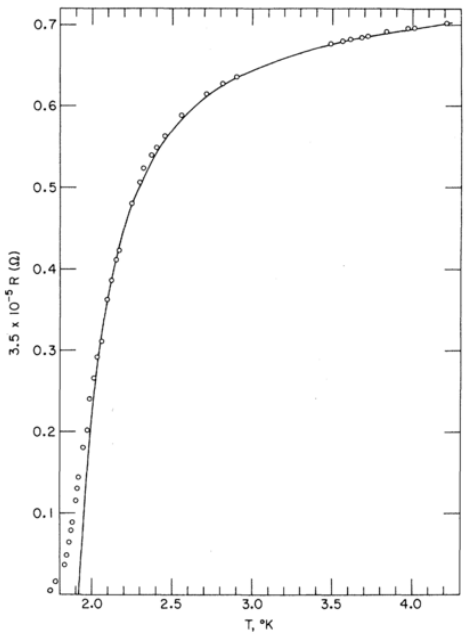

Figure 1.3: *Resistance data from Strongin et al. paper ([21]). If compared with the sharp transition of figure 1.1, it is clear how in these granular aluminum films the transition region is strongly broadened.*

Glover [18] firstly and a little later Strongin et al. [21] showed for the first time, in the late sixties, that for some granular superconducting samples, it was possible to experimentally observe a smoothening of the otherwise sharp resistance transition from the normal to the superconducting phase. What they measured was an unexpected widening of the transition region; as said before in this chapter, Ginzburg calculations predicted the transition to occur within an extremely narrow interval of temperatures. All the previous experiments indeed confirmed this theoretical estimation, as shown in figure 1.1. In systems where fluctuations have a significant role, though, the possibility to see some smearing effects arises.

The resistance measurements performed by Glover on amorphous bismuth samples, indeed showed an anomalous decrease in resistivity before the transition temperature in a range of a few mK. Later, Strongin et al. noticed a similar behaviour in granular Al films.

As seen in fig. 1.3, the sharp transition expected is effectively smoothened, leading to a different behaviour around T_c. The fit, solid line in the figure, is carried out with a function of the form $R/R_N = (1 + \epsilon_0/\epsilon)^{-1}$, where $\epsilon = (T - T_c)/T_c$ is the reduced temperature and ϵ_0 is its value when $R = \frac{1}{2}R_N$.

As will be explained in section 2.2, this is in a very good agreement with the Aslamazov-Larkin microscopic theory of paraconductivity [17].

The resistance (or equivalently the conductivity) is not the only physical

quantity that is affected by fluctuations. A similar effect of smoothening is indeed observed in at least two other superconductor characteristics: the heat capacity and the energy gap in the density of states.

The behaviour of heat capacity of a pure superconductor in proximity of its critical temperature is one of the main features of these kind of materials and is strictly connected to the presence of the gap in the DOS.

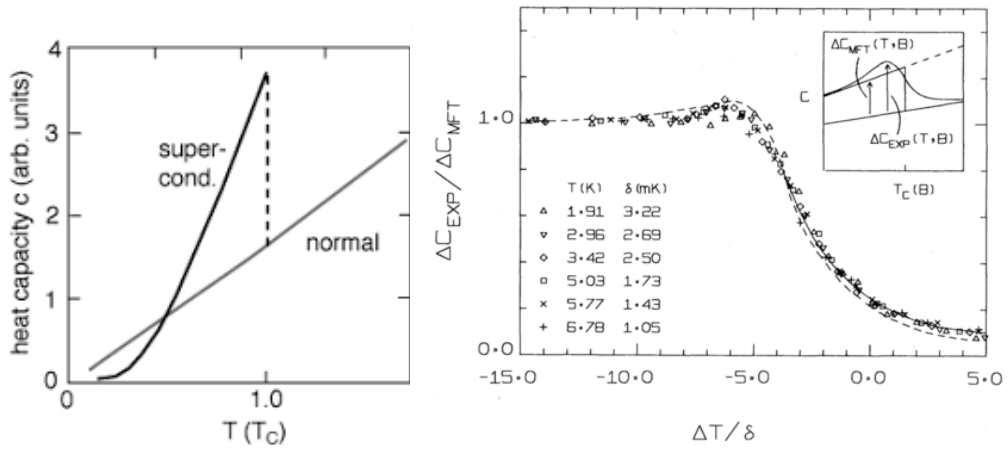

(a) *Scheme of the heat capacity jump in a pure type-I superconductor*

(b) *Heat capacity jump vs temperature: the ratio of the measured value on the MFT one is displayed*

Figure 1.4: *Heat capacity jump ΔC vs T in the ideal case (a) and its smoothening (b)*

It shows, as highlighted in figure 1.4(a), a typical jump ΔC at $T = T_c$, separating the metallic phase, with its linear growth, and the superconducting one, characterised by an exponential behaviour.

This is not the case, anyway, for the whole new group of materials in which fluctuation phenomena have great influence. Figure 1.4(b) shows many experimental data showing this effect. The ratio of ΔC_{Exp} to the jump predicted by mean field theory and verified in type-I superconductors is plotted against $T - T_c$.

We can see that deep inside the superconducting region, the ratio is almost fixed to unity, while approaching the critical temperature it has a little peak and then reaches a very small value. This reveals a decreasing of the sharpness of the jump, as shown in the inset in the picture.

A theoretical explanation of this effect is indeed possible taking into account also fluctuations in termodynamic quantities.

To conclude this section, we will describe two phenomena belonging to the precursor effects' category:pseudogap and paraconductivity.

Pseudogap consists of a suppression of the one-electron density of states around the Fermi energy due to the persistence of fluctuating Cooper pairs above the critical temperature.

Experimental data come from tunneling current measurements and have been refined through years. Cohen et al. achieved, among the firsts, some

good density spectra above T_c in a Josephson junction system where two superconducting layers, one in its *flcutuational* phase and the other deep into the superconducting state, are connected through an insulator. In the case here reported, [24], the first layer was composed by granular aluminum, the insulating material was aluminum oxyde, while the superconductor was lead or indium.

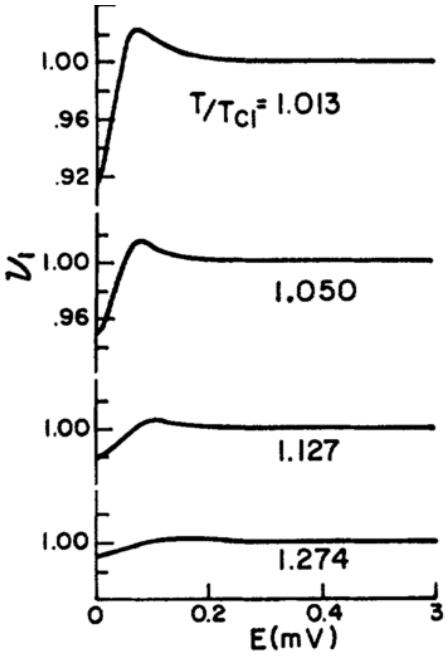

Figure 1.5: *DOS data from Cohen et al. article ([24]). It can be easily observed the dip at the Fermi energy and its decrease with rising temperature.*

In figure 1.5, we can see that a pseudogap-like behaviour exists up to relatively high T/T_c ratios of 1.274. The closer T/T_c to unity, the deeper the dip at the Fermi energy of the Density of States, while at $T < T_c$ the entire gap is restored, together with coherence peaks. We must highlight here that coherence peaks are indeed a hallmark of the superconductive phase. The formation and the subsequent condensation of Cooper pairs, indeed, gives to the system an order, which displays in peaks in the single-electron DOS. Therefore, the combination of the energy gap and of the coherence peaks in the electronic spectrum highlight the presence of superconductivity. The sole energy gap, thus, is not a sufficient evidence of the superconducting phase.

Authors observe that the temperature range in which these anomalies in the electronic spectrum are measured is the same in which charge transport is affected by fluctuations, too.

In the last fourty years a great improvement in microscopical techniques, and specifically in Scanning Tunneling Microscopy and Scanning Tunneling Spectroscopy (STM and STS), lead to experimental pseudogap data of a very high quality.

A more recent work by Sacépé et al. [23], shows the presence of pseudogap

in a conventional superconductor, ultrathin films of TiN, in the proximity of the transition to the insulating state (SIT).

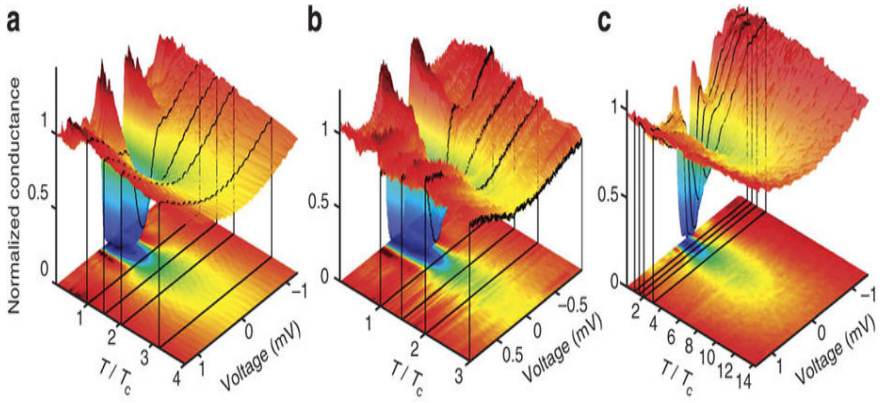

Figure 1.6: *Conductance of three different TiN thin films, measured by Sacépé et al. reported in [23]. A strong pseudogap feature is clearly measured in all the three samples, up to high temperatures.*

In figure 1.6 the conductance spectra of three samples (namely TiN1 (a), TiN2 (b) and TiN3 (c)) is shown up to many times the critical temperature, always displaying pseudogap features. We can clearly see that below T_c the energy gap is combined with the presence of coherence peaks, thus indicating superconductivity. The strong surviving of the pseudogap above T_c seems to be connected to the proximity of a transition to the insulating phase and to the low dimensionality of the system.

The last phenomenon that will be presented in this section is paraconductivity. We already discussed the effects of fluctuations in resistance as an example of the smoothening of the superconductive transition. Now we will briefly show how the same behaviour can be seen as a precursor effect, also. Since resistance is reduced at $T > T_c$ from its normal value, an increase of the conductivity in the sample, above the transition, is observed. This increase is singular in the reduced temperature, thus diverges at the transition, leading to superconductivity. Consequently, we can consider this phenomenon effectively as a precursor one, as it discloses superconductive features at temperatures higher than the critical temperature.

1.2 Superconductor Insulator Transitions (SIT)

Disorder in electronic systems has a dramatic effect; in normal metals it can lead [32] to a Metal-Insulator Transition (MIT) due to the phenomenon known as Anderson localization [33]. In the presence of impurities, the electronic motion is indeed disturbed and, with increasing disorder, it can lead to an insulating phase. This defects-driven transition from metal to insulator has been studied for the last 60 years.

Nevertheless, when the metal happens to be a superconductor, it is shown through the so-called Anderson's theorem [53], that disorder poorly affects the critical temperature and the energy gap. As mentioned in the previous section,

though, experimental evidence of critical temperature reducing is observed in dirty low-dimensional systems. This means, as formerly said, that fluctuations of the order parameter have an important role in these materials.

A Superconductor-Insulator Transition (SIT) due to quantum flucutations is expected to occur at $T = 0\ K$ for a certain value of impurity concentration and at very small film thickness ([34]). It is mainly in two-dimensional systems that this transition is indeed observed ([38],[39],[40]), as fig.1.7 shows, since superconductivity is weaker in 2D media and localization is stronger.

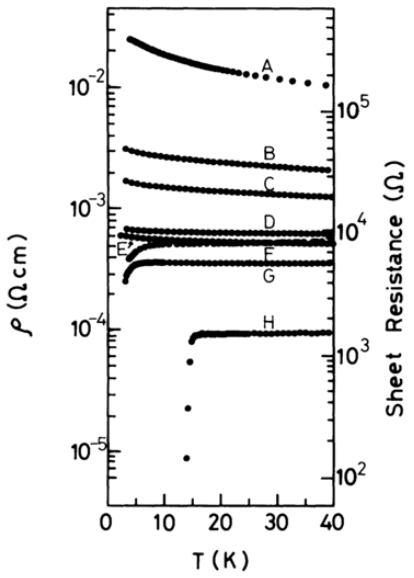

Figure 1.7: *Resistivity curves for different disorder intensities. The most disordered samples (D-A) do not show a transition to the superconducting phase, thus their critical temperature is zero. Samples E-H, instead, show a non-zero T_c, but its value decreases with increasing disorder. It is noteworthy the decreasing of normal state resistivity for decreasing disorder (A→H).*

While in metals the only carriers that can localize are electrons, in superconductors a question naturally arises on the action of disorder: it firstly destroys Cooper pairs and then localize bare electrons or the Cooper pairs are driven, altogether, to localization?
The answer is that both these scenarios are possible and experimentally observed.

The order parameter ψ is a complex value: $\psi = \sqrt{\Delta}e^{\imath\phi}$, where Δ is the energy gap. Consequently fluctuations can affect either the amplitude or the phase of ψ, leading to the two different scenarios mentioned above.

The first one, known as *fermionic* scenario is observed in homogeneously disordered systems and it ascribes the transition to fluctuations in the amplitude of the order parameter. If instead the transition happens because of fluctuations of the phase ϕ of the order parameter, the second picture of a *bosonic* framework arises. This usually happens when the system is strongly disordered or granular.

As mentioned above, experimental results are found in agreement with both the thoeretical frameworks proposed. On the one side, some electronic density

of states measurements ([41],[42]) showed that the energy gap vanishes at the SIT, thus suggesting that Cooper pairs break-up at the transition. On the other hand, though, transport properties exhibit a scaling behaviour consistent with the one predicted in the bosonic hypothesis [43],[44].

A computational work by Bouadim et al., [20], took into accout the fermionic hamiltonian of the Hubbard model, eq.1.1, where c and $c^\dagger$ are the annihilation and creation fermionic operators, t is the hopping constant between neighboring sites R and R', V_R is a random potential and $|U|$ is the on-site attraction generating the superconducting phase

$$\hat{H} = -t \sum_{\langle RR' \rangle, \sigma} (c^\dagger_{R\sigma} c_{R'\sigma} + c^\dagger_{R'\sigma} c_{R\sigma}) - \sum_{R\sigma} (\mu - V_R) n_{R\sigma} - |U| \sum_R n_{R\uparrow} n_{R\downarrow}. \quad (1.1)$$

In their simulations, the authors included thermal and quantum fluctuations, together with inhomogeneities in the amplitude of the order parameter. This led, through quantum Monte Carlo (QMC) calculations, to the study of several single particle spectra, with varying temperature and disorder strength (V).

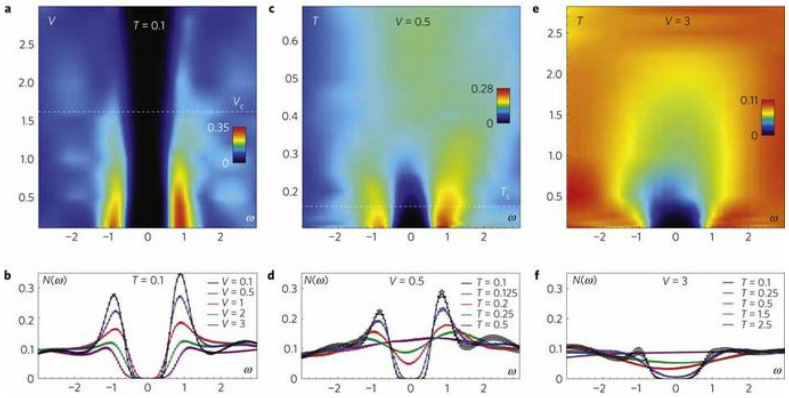

Figure 1.8: *Upper row: $N(\omega)$ maps for different T and V values. In the first panel on the left, the temperature is kept constant while disorder (V) is increased: the gap in the DOS is always observed (black region). In the central panel an intermediate disorder value $V = 0.5$ is used, while varying temperature: beyond a certain T value, both the gap and the coherence peaks vanish, thus indicating the insulating phase. In the last panel, V has a quite high value, and at all temperatures no coherence peaks are shown: this panel displays an insulator.In the lower row spectra are compared in the same conditions of the upper row maps.*

In figure 1.8 some of the results of [20] are shown. In the left panels, the electronic spectrum is displayed at a fixed temperature of $T = 0.1\ K$ and at increasing disorder. It is possible to observe how the energy gap persists at all V values, but the coherence peaks are lost as disorder is increased. At the centre of the figure, a study of temperature dependence of the density of states at a fixed disorder value $V < V_c$ is performed. While the coherence peaks, in red, vanish at the critical temperature, the pseudogap strongly persists well above the transition. In the upper panel, the blue region around zero coincides with

the energy gap (dark blue) or the pseudogap, depending on the temperature. We can, then, observe the pseudogap feature even above the transition temperature of 0.2 K, at which, instead, the coherence peaks vanish. Lastly, on the right figure, a similar investigation is pursued in a different disorder regime, above the critical value V_c. It is noteworthy the absence of coherence peaks at any temperature, proving the insulating phase. Furthermore we can observe how the low temperature energy gap evolves to a pseudogap as temperature is increased.

Further efforts, [54], have been spent in order to understand by computational tools the nature of the transition. In the cited paper, it is shown that with increasing disorder the amplitude of the order parameter begins to be rather inhomogeneous, forming some puddles of $\Delta(R) \neq 0$ embedded in an insulating phase where no pairing is observed. It is then argued that at this disorder values, also phase coherence is destroyed by fluctuations, thus the different locally superconducting regions, whithin which coherence is still present, have no accord between them, leading to an overall insulating phase (fig.1.9).

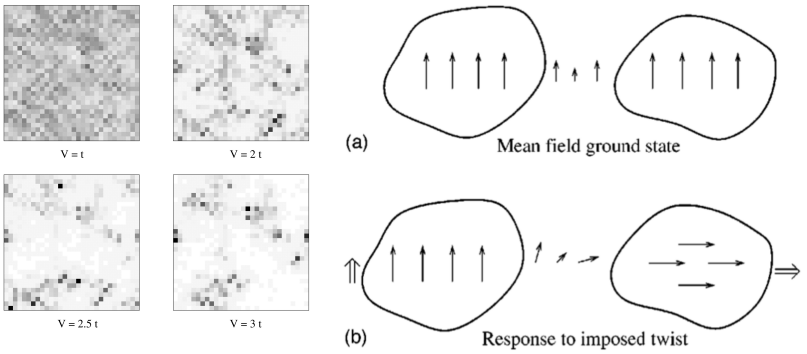

Figure 1.9: *On the left: $\Delta(R)$ maps for different disorder strengths show evolution from an homogenous distribution to isolated puddles; on the right: schematic explanation of the coherence loss between different superconductive regions*

As shown in the right-upper panel of figure 1.9, amplitude fluctuations could be uneffective in destroying phase coherence, when acting alone, while when to these phase fluctuations are added, the effect is of changing the order parameter's phase in the regions where its amplitude is lower, with a little energy cost, and thus lead to a total loss of phase ordering, as displayed in the lower panel.

1.2.1 Bosonic picture

As stated above, the bosonic scenario suggests that Cooper pairs survive the transition and still exist in the insulator. Nonetheless, their persistence at the insulating side of the transition cannot lead to conducitivity, as the granular structure of the materials forces the Cooper pairs to localize in grains or puddles whithout any coherence between them. As a consequence, in this scenario the loss of superconductivity cannot be ascribed to fluctuations in the amplitude of the order parameter, hence to the break-up of Cooper pairs, but rather to phase inhomogeneities, destroying the superconducting stiffness.

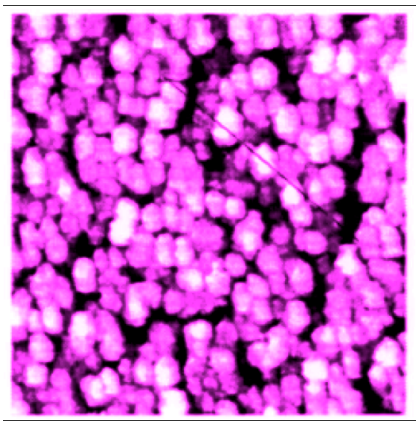

Figure 1.10: *The granular structure of a Pb film, obtained thorugh STM*

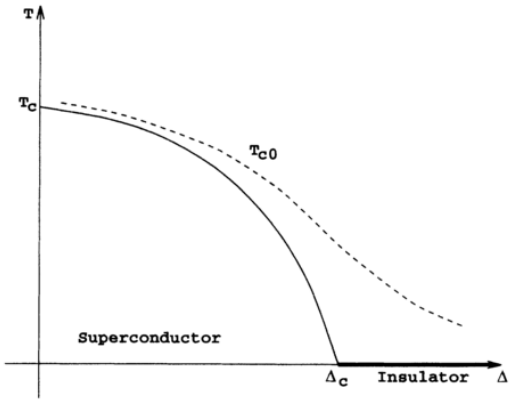

Figure 1.11: *SIT phase diagram, reported from [37]. Dashed line: temperature T^* at which Cooper pairs begin to form. Solid line: critical temperature T_c, at which resistance goes to zero. At $T = 0$ and $\Delta = \Delta_c$ the transition from superconductor to insulator sets in.*

In figure 1.11 the phase diagram of a two-dimensional amorphous superconductor is shown, as a function of temperature and disorder Δ. The dashed line represents the critical temperature at which Cooper pairs begin to bind together. It is possible to appreciate how this curve diverges from the transition temperature as disorder is increased. The Superconductor-Insulator transition sets in at $T = 0$ at a certain critical disorder Δ_c.

In the bosonic hypothesis, the critical temperature at which Cooper pairs begin to bind, i.e. the temperature below which $\Delta > 0$, is weakly affected by disorder, which is much more effective in generating fluctuations in the phase. It is possible to observe in some experimental R vs T curves, like the one in figure 1.12, how this is indeed the case for some granular samples, where a sharp change in the resistance behaviour is measured at a fixed temperature T^*, where pairs are formed, not varying with increasing disorder.

On the other hand, though, charge transport at $T < T^*$ is quite compli-

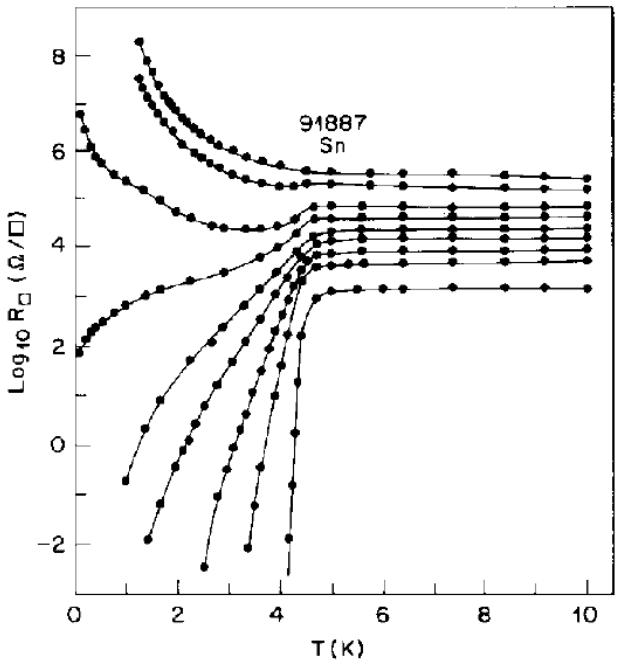

Figure 1.12: *Tin resistance data for increasing disorder; the knee at which there is a change in the behaviour always happens at the same temperature.*

cated by phase fluctuations, decreasing the conductivity with increasing disorder and pointing to an insulating phase, cahracterized by a quasiparticle tunneling transport. Charge transport between incoherent contiguous grains may occur through Josephson tunneling. Since Cooper pairs are made of two bound electrons, their tunneling probability is roughly the square of the bare electron one. Consequently electronic quasiparticle hopping between neighboring grains is preferred with respect to Cooper pairs tunneling current. For the same reason, these granular superconductors have a negative magnetoresistance. The effect of the magnetic field, in fact, is of destroying Cooper pairs, thus yielding an increase in charge current, as single electrons have a greater *mobility* in these systems.

Concerning spectral features, a persisting energy gap in the insulating phase is expected, since $\Delta \neq 0$ there and Cooper pairs are still bound together. This feature is confirmed by many tunneling spectroscopy conductance experiments, showing a hard gap for some temperature ranges followed, generally, by a pseudogap.

In order to give a suitable theoretical background to the bosonic hypothesis, in the late eighties Fisher et al. [31] introduced a complete formalism with the aim of studying lattices of bosons in the presence of disorder, represented by a random potential. A little later, [35], the application of the formerly introduced formalism to the problem of a condensate of bosonic Cooper pairs was pursued in more detail. In accord with the persistance of Cooper pairs in the insulating phase, the authors stated that the SIT could be described within a framework of $2e$-charged bosons moving in a random potential. In this theory,

the competition between kinetic energy and repulsive interaction, together with the random potential is responsible for the transition. The first, in fact, has a tendency to delocalize particles and reduce phase fluctuations and thus lead to Cooper pairs' condensation, while the second enhance on the contrary particles localization. Then, when the density degrees of freedom are somewhat frozen, the conjugate quantum d.o.f., namely the phase, fluctuates more widely.

The hamiltonian describing this system is:

$$\hat{H} = -\sum_i (-J_0+\mu+\delta\mu_i)\hat{N}_i + \frac{1}{2}V\sum_i \hat{N}_i(\hat{N}_i-1) - \frac{1}{2}\sum_{i,j} J_{i,j}(\hat{\phi}_i^\dagger\hat{\phi}_j+\hat{\phi}_j^\dagger\hat{\phi}_i). \quad (1.2)$$

Where ϕ is a bosonic field operator, satisfying the canonical commutation rules, $\hat{N}_i = \hat{\phi}_i^\dagger\hat{\phi}_i$ is the number operator, counting the number of particles in a determinate state, $J_{i,j}$ is the hopping strength between sites i and j ($J_0 = \sum_{i,j} J_{i,j}$), μ is the chemical potential and $\delta\mu_i$ is a random on-site potential with zero mean. V is the strength of the on-site soft core repulsive potential. The distribution of $\delta\mu_i$ could be either uniform or gaussian and it depends on the value of the disorder Δ.

Since the transition is expected at zero temperature, the universal scaling cannot be found as a power law of $T - T_c$ and a parameter δ, measuring the distance from the transition at $T = 0$ must then be added. According to the theory, then, the coherence length diverges at the transition as $\xi \sim \delta^{-\nu}$; furthermore a characteristic frequency Ω ruling all energy and temperature scales arises in this system, vanishing at the transition as $\Omega \sim \xi^{-z} \Rightarrow \Omega \sim \delta^{z\nu}$.

According to Fisher et al., between bosons (i.e. Cooper pairs) and vortices in the bosonic wave-function a dual relation exists, at the transition. Hence, while in the superconducting phase Cooper pairs Bose-condense, leading to zero resistance, and vortices are localized, in the insulating phase, on the contrary, bosons are localized, impeding conductivity at all, whereas vortices proliferate and condense. The transition is the point at which bosons and vortices exchanghe their roles, and thus they are both mobile, leading to a finite resistance. Theoretical calculations, indeed, give a conductivity behaviour which remains finite, at the criticality, when the temperature is lowered to zero: $\sigma(T, \xi = \infty) \sim T^{(\mathcal{D}-2)/z}$.

In the two-dimensional case, the resistance per square $R_\square$, when expressed in units of the quantum of resistance $h/4e^2$, is a pure number. Renormalization group analysis shows that this number is, similarly to the critical exponents, a universal value, not depending on the microscopic nature of the sample, but only on the universality class it belongs to [37],[35]. Experiments on Josephson junctions arrays, through which is possible to describe granular superconductors, show effectively to approach a finite universal resistance at $T \to 0$, [55].

1.2.2 Fermionic picture

At the opposite side of granular systems, there are homogeneously disordered materials, the difference being in the typical lengthscales over which disorder displays. In granular systems, impurity's distribution is strongly inhomogeneous, forming grains, while at the opposite side stand homogeneous dirty superconductors, where impurities are distributed homogeneously in the sample.

In granular films (fig.1.12), when disorder is increased, the temperature range over which R reaches zero may become a few Kelvin wide. On the contrary, in

homogeneous samples a rather direct superconductive transition is observed at all disorder values $\Delta < \Delta_c$. In figure 1.13 it appears clearly this behaviour for decreasing film thickness of homogeneous bismuth samples: at $t > t_c$ the transition occurs in a narrow temperature range. At $t < t_c$, instead, the transition to the insulating phase takes place.

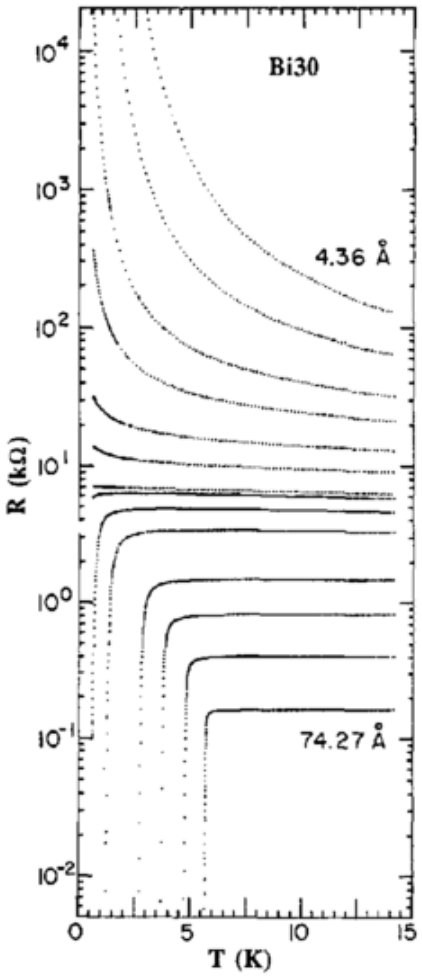

Figure 1.13: *Sheet resistance vs temperature for homogeneously disordered Bi films; data from [57]. Decreasing the film thickness (lower to upper curves), the critical temperature decreases and, at some critical thickness t_c, it vanishes. Remarkably, the behaviour at $t > t_c$ always shows a quite sharp transition, if compared to other similar curves from granular films (see fig.1.12).*

Another interesting quality strongly different from granular systems' characteristics is the decreasing of the transition temperature with increasing disorder. We can observe this feature both in figures like 1.13 where the transition knee is moved towards the left side of the x-axis and in graphs like the one of figure 1.14, where the critical temperature is plotted against the sheet resistance of the film in the normal state (clearly the bigger $R_\square$ the stronger the disorder).

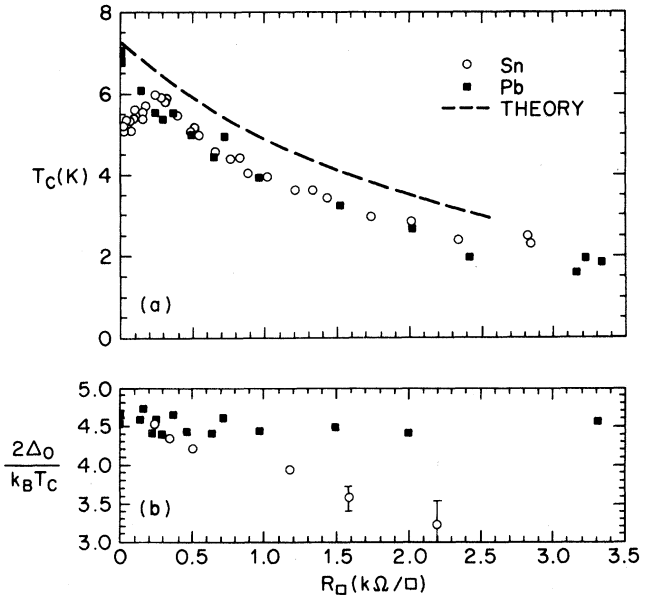

Figure 1.14: *Upper panel: T_c vs $R_\square$ for homogeneous Pb and Sn samples; Lower panel: Δ/T_c vs $R_\square$ for the same samples. The constant ratio, at least for the lead sample, indicates that together with T_c also the energy gap decreases and eventually vanishes.*

From the bottom panel of figure 1.13 another remarkable feature arises: the energy gap reduces roughly at the same rate as the critical temperature, in contrast with the observation of energy gap inside the insulating phase for granular superconductors.

According to these observations, Finkel'stein proposed that the mechanism relying behind the SIT in homogeneously disordered superconducting films is driven by the amplitude of the order parameter, related thus to the suppression of the gap and of T_c with increasing disorder. In this picture then is the competition between the phonon-mediated attraction between electrons and the Coulomb repulsion that drives the transition. While the first is substantially independent on the disorder strength, impurity scattering considerably reduces the electronic screening, making the Coulomb repulsion more effective. Since the binding energy of the Cooper pairs is roughly the sum of these two contributions, when disorder is enhanced, there will be a certain point beyond which electrons' attraction does not exceed their repulsion anymore, thus leading to pairs' breaking.

After destroying Cooper pairs, disorder drives single electrons to a weak localization, bringing the system to an insulating phase.

Since the main parameters of the Fermi liquid are invariant under the varying of the film thickness, while the sheet resistance obviously is not, it is argued that the variation of the critical temperature with $R_\square$ must be ascribed to the sole interplay of Coulomb repulsion and impurities scattering. Consequently, the expression of $T_c(R_\square)$ is researched considering only these interactions, together with renormalization group's equations for the electron gas. The reduction of

the transition temperature with respect to the bulk one is expressed in eq.1.3:

$$\frac{T_c}{T_{c0}} = e^{-\frac{1}{\gamma}}\Big[(1+\frac{\sqrt{(e^2/4\pi^2\hbar)R_\square}}{\gamma-(e^2/8\pi^2\hbar)R_\square})(1-\frac{\sqrt{(e^2/4\pi^2\hbar)R_\square}}{\gamma-(e^2/8\pi^2\hbar)R_\square})^{-1}\Big]^{1/\sqrt{(e^2/\pi^2\hbar)R_\square}}. \tag{1.3}$$

Where $\gamma = \frac{1}{log(T_{c0}\tau)}$, with τ as the free path time. The behaviour of this expression is linear with the sheet resistance for $(e^2/4\pi^2\hbar)R_\square \leq |\gamma|^3$, to which follows a slow-down in the decrease of T_c, that vanishes at $\sim \gamma^2$ and thus at a value which is material-dependent, being function of the lifetime τ. The only fitting parameter of this equation is γ and a very good agreement is found for Mo-Ge data, whose comparison with the theoretical prediction is showed in figure 1.15.

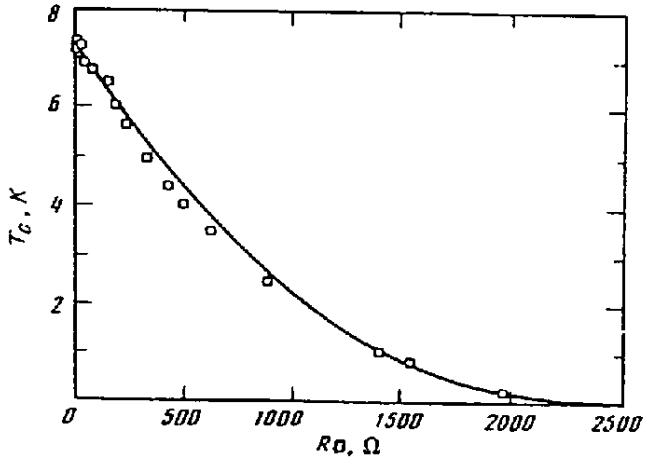

Figure 1.15: *T_c vs $R_\square$ for Mo-Ge data (empty circles) compared with theoretical prediction (thick line)*

We can notice the initial linear decrease, followed by the predicted slow-down and the final total vanishing of the critical temperature.

1.3 NbN ultrathin films

The main focus of this thesis is finding a theoretical counterpart to the STS conductance data obtained on niobium nitride ultrathin films in [2]. The thinnest of the samples studied in the cited paper show in fact many anomalies in charge transport and spectral properties, when related to their morphological features.

Niobium nitride is a s-wave superconductor with a tridimensional fcc structure like the one sketched in fig.1.16. It thus has four niobium atoms per unit cell, each of them carrying five electrons in the outer shell, as Nb electronical structure is $[\mathrm{Kr}]4d^45s^1$, for a total carrier number per cell of 20. Its lattice parameter is $a = 4.413$ Å, giving a carrier density $n = 2.33 \times 10^{29} m^{-3}$.

As a conventional superconductor, niobium nitride has a quite large transition temperature of $\sim 16\ K$ and a small coherence length $\xi \leq 5\ nm$. Further-

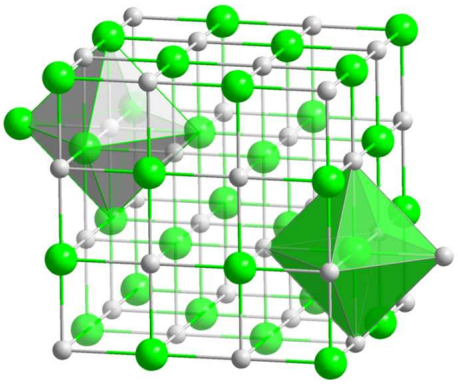

Figure 1.16: *FCC structure of niobium nitride, in green Nb and in white N atoms*

more it has a large penetration depth. These characteristics allow the production of thin films, even two-dimensional, with a transition temperature of typically a few Kelvin. Moreover, NbN films have good mechanical and chemical properties. All these features make niobium nitride an excellent compound to study many physical phenomena in low-dimensional systems.

The films studied in this work are only a few nanometers thick and substantially two dimensional, since their coherence length is larger than the sample thickness. They have been produced in Karlsruhe Institute of Micro and Nanoelectronic Systems laboratories using the magnetron sputtering of a niobium target in a Ar+N_2 atmosphere; the substrate used was the optically polished side of sapphire crystals. N_2 partial pressure and deposition rate were optimized in order to have the highest transition temperature [58]. Figure 1.17 displays a TEM image of a sample of thickness $t = 2.33\ nm$.

The film shown in this image is composed by nanocrystal of typical size $d \sim 2 \div 5\ nm$.

Among the experimental parameters of some importance, certainly thickness and aging have the main roles. It was indeed found in studies on the transition temperature that decreasing film thickness and after time cicling T_c reduced from its original value. Together with critical temperature lowering, normal resistance enhancement was measured, thus making of these two parameters good tuning tools of the SIT.

Remarkably it appears from experimental data that thinner films have unexpected behaviours in some measured physical quantities.

While the thickest of the films showed features in good agreement with the expected behaviour, the thinnest and aged samples exhibited anomalies in paraconductivity, electronic inhomogeneities and pseudogap. These phenomena are not in accord with the formal characteristics of the samples: two-dimensionality and homogeneity. As will be illustrated in the following, paraconductivity displays a behaviour that can be explained formally by a zero-dimensional Aslamazov-Larkin theory. Spectral properties, instead, show inhomogeneities on a lengthscale different from the one highlighted in morphological maps. Moreover, these characteristics belong to different SIT frameworks. Paraconductivity is understandable in a fermionic scenario, as we already stressed that transport,

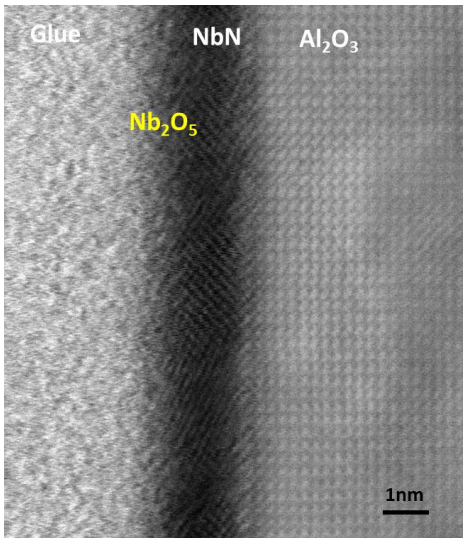

Figure 1.17: *TEM image of a NbN sample; the presence of a niobium oxyde on top of the film is argued from AFM data and chemical analysis*

in bosonic systems, is characterised by quasiparticles tunneling. On the other hand, pseudogap is definitely a bosonic hallmark.

In order to have a better understanding of these strange properties, we will briefly report the main results obtained in [2].

1.3.1 Pseudogap Inhomogeneities

The samples were measured by Scanning Tunneling Microscopy with the aim of confirming their overall homogeneous morphology. The topographic maps show, as reported in fig.1.18, that the surface has some small inhomogeneities, corresponing to the cristallites composing the whole crystal, of a dimension $d_c \sim 5nm$.

From Scanning Tunneling Spectroscopy maps, it was possible to display the gap $\Delta(x, y)$ on the same areas studied with topographic data. These measurements were performed at a temperature $T = 300\ mK$, well inside the superconducting phase, as the presence of the peaks in the dI/dV graph confirms; the value of the gap was taken to be the peak-to-peak distance, in energy, from those same dI/dV curves. In figure 1.19, always from the original paper, we show the STS map and the dI/dV measurements.

Inhomogeneities in the electronic spectra have already been observed in some experiments ([25],[26]), thus their presence in this map is not surprising. The fact which is instead astounding is that no correlation exists between the energy gap and the morphological inhomogeneities. At a first glance the areas where a significant difference in the spectrum is observed seem to be much larger than the cristallites' size obtained in the STM map of fig.1.18. Further analysis showed no correlation at all between morphological and spectral inhomogeneities.

The investigation on the radial profile obtained from the autocorrelation map allowed to estimate these regions' dimension, L_i, as the distance of the

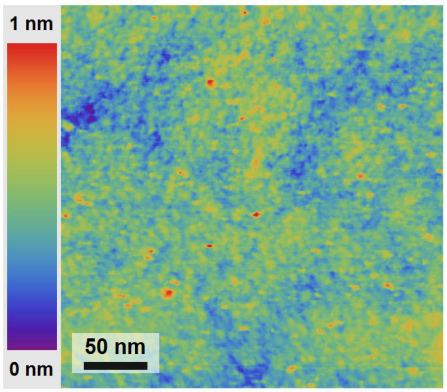

Figure 1.18: *Topographical map of the sample X_0 of thickness $d = 2.14nm$, with critical temperature $T_c = 3.8K$.*

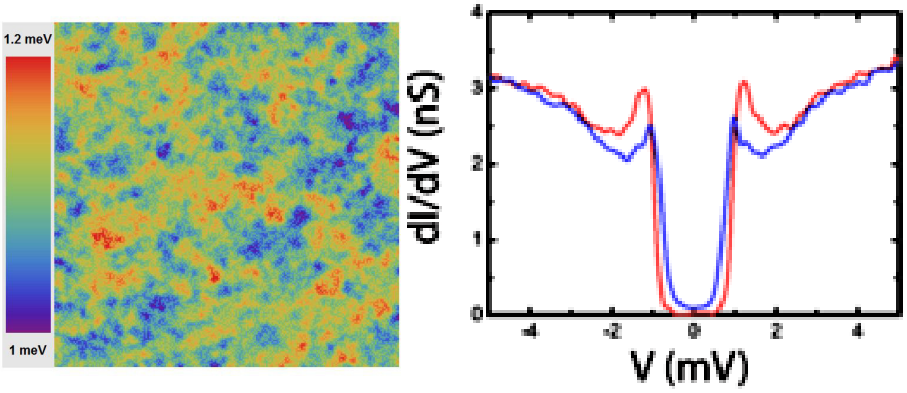

(a) *STS map of sample X_0 at T =* (b) *dI/dV curves in the higher (red) and lower* 300 mK. *It is possible to observe the dif-* *(blue) gap regions*
ferent gap regions. In red the high-gap ar-
eas, while in blue the low-gap ones.

Figure 1.19: *Gap measurements on the sample named X_0, 2.14 nm thick $T_c =$* 3.8 K

first peak in figure 1.20: L_i value is roughly an order of magnituded larger than the cristallite's size, d_c.

More precisely, these areas (to which we will refer as *supergrains*) show a typical dimension of $L_i \sim 100\ nm$ and a distance between contiguous supergrains of $L_i/2$.

At a temperature $T = 4.2\ K > T_c$ a pseudogap-like spectrum is observed in conductance data from STS. Similarly to the measurements performed inside the superconductive phase, STS maps were obtained at this temperature, showing inhomogeneities over regions compatible with the ones found at $T < T_c$.

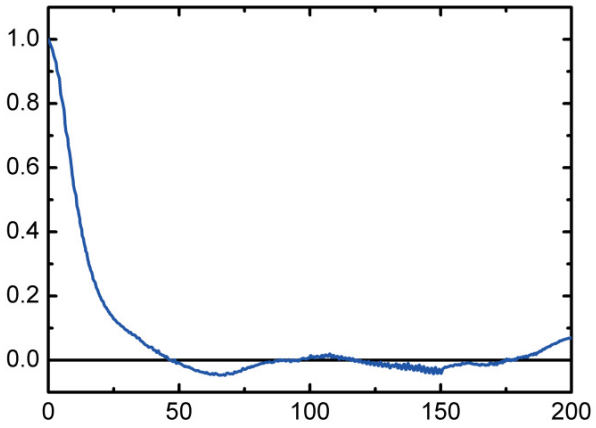

Figure 1.20: *Radial correlation function, as extracted from autocorrelation map of STS data*

Again the correlation map of the STS data above and below the critical temperature was studied and gave good agreement between energy gap and pseudogap inhomogeneity regions, allowing the extraction of supergrains' size in the normal phase. The supergrains dimension at $T > T_c$ was found in good agreement with the size L_i measured in the superconductive phase.

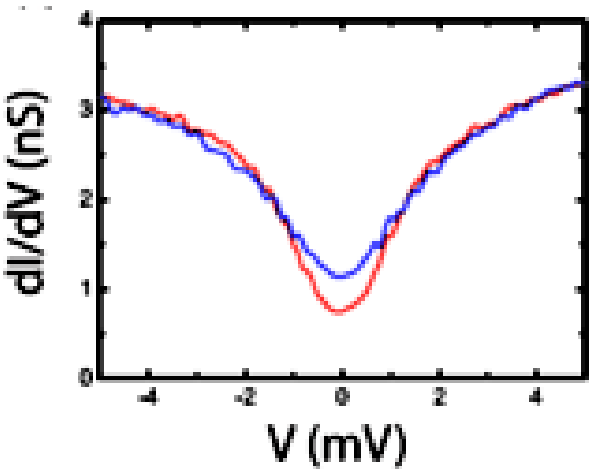

Figure 1.21: *Comparison of pseudogap spectra at $T = 4.2\ K$: in red a curve measured in the high-pseudogap supergrains, while in blue one obtained in low-pseudogap regions*

The hypothesis of a locally higher critical temperature, in order to explain this increase in pseudogap, is discarded as the dI/dV curves in figure 1.21 show no peaks.

A similar study has been made on the same samples at a temperature inside the $0D$-paraconductivity regime ($T = 7\ K$), giving results in good agreement with the existence of a pseudogap even this far from the transition. A larg pseudogap, measured even at temperatures at which one would expect none of this feature, is unexpected in these kind of samples. The aim of this thesis is, indeed, to explain this behaviour by means of the same mechanism driving the paraconductivity anomalies discussed in the next section.

The good correlation between the supergrains in the pseudogap phase and in the superconducting one, together with the unchanging dimension of the supergrains with temperature, suggests that a common mechanism rules these inhomogeneities below and above T_c.

For thicker samples ($d \geq 2.3\ nm$, $T_c \geq 0.3T_{c0}$) these effects are less significant, decreasing with thickness.

1.3.2 Paraconductivity anomalies

As mentioned above, another surprising feature of NbN ultrathin films comes from electrical transport measurements. In first place, resistance measurements show for all samples, as indeed expected, curves that indicate fluctuations' effects to be relevant in the systems studied. The smearing out of the sharp superconducting transition is clearly observable in figure 1.22, where resistance per square is plotted against temperature.

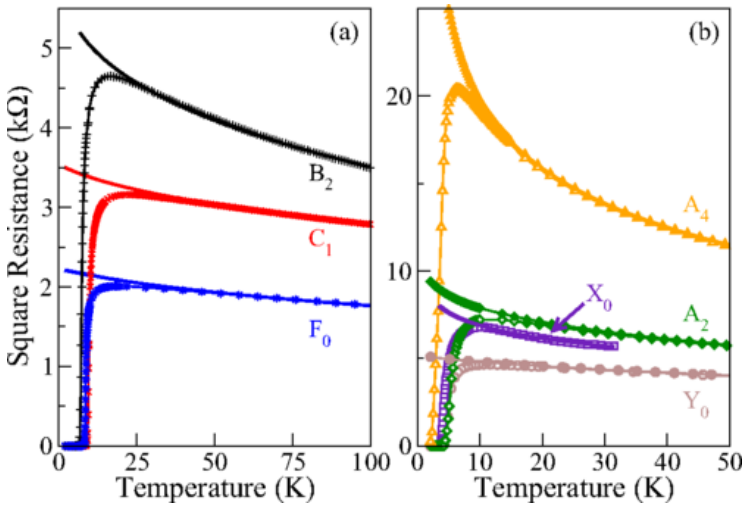

Figure 1.22: *Square resistance of the samples studied. (a): Thicker samples are here reported, with the fit of the normal resistance at temperatures $T < T_c$ (solid lines). (b): thinner samples data, here the normal phase resistance is experimentally observed using a strong magnetic field in order to destroy the superconducting states at temperatures $T < T_c$*

Subsequently, the excess conductance per square $\Delta\sigma(T) = \sigma(T) - \sigma_N(T)$ is measured and plotted with respect to $\epsilon \equiv log(T/T_c)$ in a log-log scale.

Figure 1.23 compares the results obtained on thicker samples with the ones mesured on the thinner ones. The first are in perfect agreement with the

Aslamazov-Larkin theoretical prediction $\Delta\sigma(T) = \frac{e^2}{16\hbar\epsilon}$ (solid light blue line) over a relevant range of ϵ values without any correction from other fluctuation effects such as the Maki-Thompson ([28],[29]) or the DOS contribution.

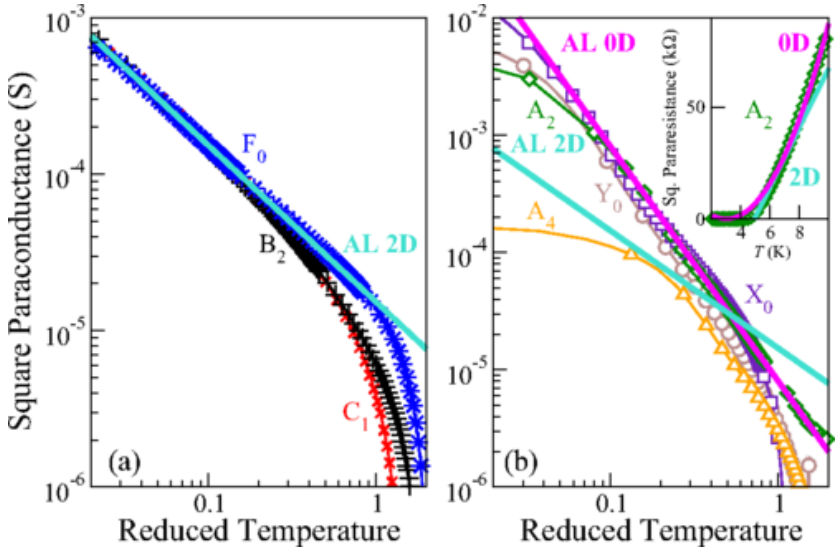

Figure 1.23: *(a):Paraconductance per square in thicker films. It is clear how the Aslamazov-Larkin prediction (light blue solid line) is in perfect agrement with experimental data over a wide temperature range. (b): Paraconductance per square in the thinnest samples. As thickness is decreased, the agreement with the theoretical prediction is completely lost. The fitting with the A-L paraconductivity obtained in the zero-dimensional limit is, instead, very good.*

For thinner samples, panel (b), instead, there's no agreement at all between the experimental data and the corresponding theoretical curve (light blue solid line), even taking T_c as a free parameter. Remarkably, a power law dependence $\sim \epsilon^{-2}$ is observed here, in agreement with results obtained in granular systems ([61],[62]), highlighting a seemingly 0D behaviour. A trial function $f(\epsilon) = \frac{0.03e^2}{\hbar\epsilon^2}$ is reported in the plot as a purple solid line, in order to evidentiate the good fitting with paraconductance data over a rather wide range of temperatures.

Even though one could argue that the inconsistency of the results with the 2D A-L prediction is due to the fact that the choice of the critical temperature plays an important role, assuming, as it is legitimate, that T_c^{0D} and T_c^{2D} are different, the curves plotted in figure 1.24 demonstrate that a 0D behaviour is always detected and seems very robust with respect to the choice of T_c. Futhermore, the figure reveals another interesting behaviour. It appears that a cross-over between the two regimes is plausible, especially according to the data coming from the higher-T_c plots. A similar phenomenon has indeed been already observed in other systems in [30] and will be discussed in detail in section 3.1.

In this last section of chapter 1, we have presented the main features of thin samples of niobium nitride and their anomalies. Particularly, we have stressed the characteristic charge transport of this material and its spectral properties too, highlighting the anomalies that raise so much interest on these films. In the next part of this work, we will propose and discuss an anomaly in the diffusion

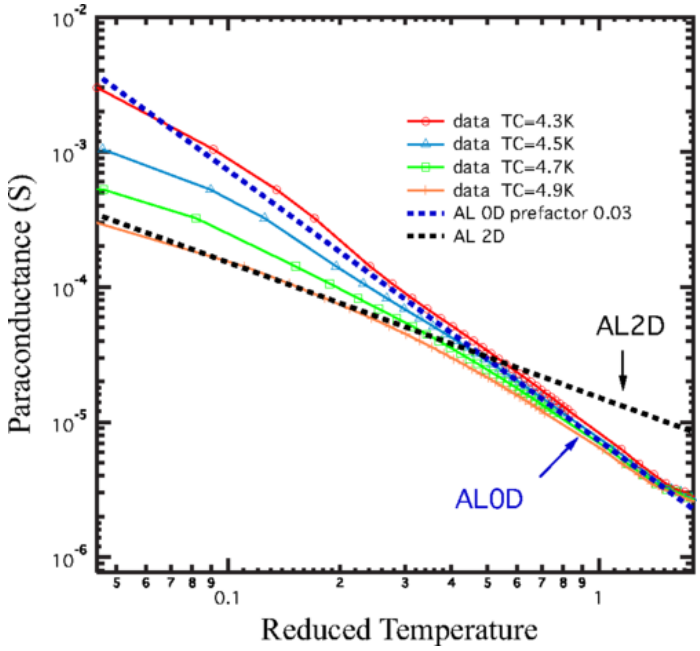

Figure 1.24: *The robustness of the 0D behaviour with different choices of T_c. Even leaving the critical temperature as a free parameter, all the curves are in good agreement with the $0-\mathcal{D}$ prediction at least at high temperature. It is worth noticing that the curves obtained via the lower T_c are closer to the zero-dimensional behaviour, while the ones obtained using high critival temperature are more similar to the $2-\mathcal{D}$ paraconductivity.*

of fluctuating Cooper pairs in order to understand and give a phenomenological explanation to these behaviours.

Chapter 2

Theory of fluctuations in superconductors

As mentioned in the previous chapter, in dirty and low dimensional superconductors fluctuations may play a relevant role. On the one hand, they are responsible of many of the effects occurring in these materials; on the other, the different *flavours* of the SIT can be explained by means of fluctuations either in the amplitude or in the phase coherence of the order parameter. It is now worth, then, to explore in more detail the physics at the microscopic scale giving rise to the phenomena presented in the previous chapter.

This chapter will be mainly focused on describing the physics generating the experimental observations of chapter 1, the reader interested in a deeper theoretical approach can refer either to the appendix A or to [4].

2.1 Fluctuations' characteristics

In the previous sections, we mentioned that all the effects beyond mean field theory are known, in physics, as fluctuations. We must underline that quasiparticles, arising from the breaking of Cooper pairs, are excitations of the mean field system, and belong to the same MFT framework. Thus, for the sake of definitness, we call fluctuations those phenomena which belong neither to the MFA nor to its quasiparticle excitation.

Deep inside the superconducting phase, for every type of superconductor, almost all the Cooper pairs are condensed in a unique state, giving rise to a macroscopical order resulting in the spectacular properties of such materials. At temperatures $T < T_c$, then, the number of Cooper pairs out of the condensate is considerably lower with respect to the total and, as a cosequence, these can be neglected. Nevertheless in proximity of the transition, $T \gtrsim T_c$, fluctuating pairs become important, in some particular materials. As already noticed, in dirty superconducting films, fluctuations have a primary role in explaining many of the weird phenomena observed. Even though these can resemble quasiparticles, a fundamental difference there exists: while for quasiparticles the excitation energy must be much larger than their inverse lifetime, for fluctuations the two can be of the same order of magnitude. For a Cooper pair, the lifetime is clearly defined as the time necessary to break the pair and decade in two bare electrons.

This time is called after Ginzburg and Landau and is denoted as τ_{GL}. Since at the transition we expect the Cooper pair to be substantially stable, when $T \to T_c^+$ the Ginzburg-Landau lifetime diverges. This assumption gives a hint on the dependence on temperature of τ_{GL}:

$$\tau_{GL} \propto \frac{1}{T - T_c}. \tag{2.1}$$

Dimensional analysis trivially gives $\tau_{GL} \sim \hbar/k_B(T - T_c)$, while comparison with the results from the microscopical theory gives the exact prefactor:

$$\tau_{GL} = \frac{\pi\hbar}{8k_B(T - T_c)}. \tag{2.2}$$

For fluctuations, a typical dimension $\xi(T)$ is defined, corresponding to the distance the two electrons can move apart from each other during the Cooper pair's lifetime τ_{GL}. We must now stress that fluctuations' motion is indeed a diffusive one, and it is thus ruled by a diffusion coefficient $D \sim v_F^2\tau$. Two opposite cases naturally appear at this point: dirty superconductors and clean ones.

For the dirty case, the time τ corresponds to the impurity scattering time. In a clean system, though, impurities do not affect electronic motion, thus the time ruling the diffusion must be a ballistic one, obtained through the uncertainty principle: $\tau \sim \hbar/k_BT$. In both cases, the total distance covered by the diffusive motion of the two electrons is given by:

$$\begin{aligned} \xi(T) &= \sqrt{D\tau_{GL}} \\ \xi_d(T) &\sim v_F\sqrt{\tau\tau_{GL}} \\ \xi_c(T) &\sim v_F\sqrt{\frac{\hbar}{k_BT}\tau_{GL}}. \end{aligned} \tag{2.3}$$

Introducing here the reduced temperature $\epsilon = log(\frac{T}{T_c}) \sim \frac{T-T_c}{T_c}$, it is easy to observe that a common dependence on $\epsilon^{-1/2}$ stands for both coherence lengths. Therefore, in both the clean and the dirty limit, $\xi(T)$ diverges at the transition, as expected.

We would like to stress here that indeed fluctuations can be treated as classical complex fields, but, rather than in a Boltzman framework, in a Rayleigh-Jeans sense. Therefore, only small fluctuation energies must be taken into account while evaluating the Bose-Einstein distribution:

$$n_B(k) = \frac{1}{e^{\frac{E(k)}{k_BT}} - 1} \simeq \frac{k_BT}{E(k)}. \tag{2.4}$$

It can be demonstrated using both the Ginzburg-Landau and the microscopical formalisms that the fluctuational energy, close to the transition, has the following expression:

$$E(k) = \alpha k_B(T - T_c) + \frac{\vec{k}^2}{2m^*} = \frac{1}{2m^*}\big[\frac{\hbar^2}{\xi^2(T)} + \vec{k}^2\big] \tag{2.5}$$

where clearly m^* is the reduced electronic mass.

2.2 Effects on conductivity

In this section we will briefly discuss the effects of fuctuations in the electrical transport of superconductors. Fluctuations of Cooper pairs above the transition temperature T_c affect conductivity in many different ways. This is not surprising, since fluctuating pairs are indeed themselves carriers of charge $2e$. Moreover they significantly modify the electronic spectrum, which is involved in the Drude formula for conductivity. It is possible to distinguish three different contributions to the normal state conductivity due to fluctuations:

- Aslamazov-Larkin paraconductivity, caused by the diffusive transport of Cooper pairs
- DOS contributions, produced by the decrease of the density of states
- Maki-Thompson corrections, purely quantum and generated by coherent scattering.

Aslamazov and Larkin paraconductivity During the sixties, after a great interest was raised on the corrections to conductivity due to fluctuations in dirty and low dimensional superconductors, Aslamazov and Larkin elaborated a theory describing one of these corrections, the so-called paraconductivty [17].

The basis of their argumentation lays in the fact that Cooper pairs are, as electrons, charged particles. For this reason, they respond to an external electric field and can thus be carriers, too. Clearly some differences exist between electronic carriers and Cooper pairs: the first being fermions and having a rather scattering-ruled motion, while the second are clearly bosons and move in a diffusive way. The study of this Cooper-channel in the electric transport thus leads to the paraconductivity term.

In the normal state, we have seen that some $2e$-charged Cooper pairs still exist and diffuse theirselves over a typical lifetime $\tau_{GL} = \frac{\pi\hbar}{8k_B(T-T_c)}$. The exact calculation of this contribution, can be carried out in a microscopical framework, using Feynman diagrams. The interested reader can find more details in [4]. In the following we will report the final results, and comment their major features.

The result for different dimensions of the system is as follows:

$$\delta\sigma_{AL} = \begin{cases} \frac{e^2}{32\xi}\frac{1}{\sqrt{\epsilon}} & 3\mathcal{D} \text{ case} \\ \frac{e^2}{16d}\frac{1}{\epsilon} & 2\mathcal{D} \text{ case,d film thickness } d \ll \xi \\ \frac{\pi e^2 \xi}{16S}\frac{1}{\epsilon^{3/2}} & 1\mathcal{D} \text{ case,S wire cross-section } S \ll \xi^2. \end{cases} \tag{2.6}$$

Where clearly ξ is the coherence length. The expression of eq.2.6 is obtained considering the simple case of an isotropic electronic spectrum and consequently conductivity loses its tensorial nature (i.e. conductivity tensor is proportional to the identity tensor).

We can notice that all the solutions are singular in the $\epsilon \to 0$ limit, thus indicating, as expected, that this correction increases approaching the critical temperature T_c. It is then worth observing that the lower the dimension of the sample, the wider the effect of paraconductivity, confirming that dimensionality has a great role in fluctuating phenomena.

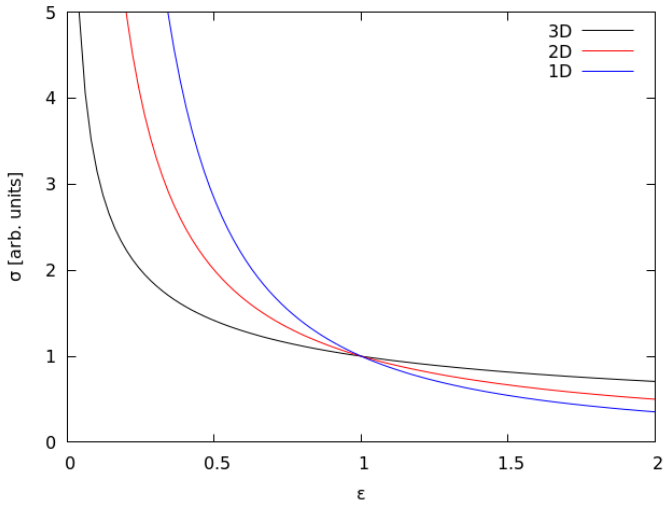

Figure 2.1: *Paraconductivity in different dimension regimes. It is interest noticing that, for $\epsilon < 1$, the lower the dimensionality, the higher the effect on conductivity.*

The two-dimensional correction due to paraconductivity shows a particular behaviour, surprisingly simple, when evaluated in its per unit square form (restoring the universal constants):

$$\delta\sigma^{2\mathcal{D}}_{AL,\square} = \frac{e^2}{16\hbar}\frac{T}{T-T_c}. \tag{2.7}$$

Since this equation does not depend on any of the microscopical details of the sample under consideration, its prefactor $\frac{e^2}{16\hbar}$ turns out to be a universal constant. This universality is suddenly lost when other dimensionalities are taken into account.

In many systems the Aslamazov-Larkin contribution appears to be the leading term in the excess conductivity measured, then assuming an important role in the description of the fluctuation contribution to charge transport.

DOS contribution The standard Drude formula for conductivity in a normal metal (eq.2.8) highlights the dependence of this quantity on the carriers' concentration n.

$$\sigma = \frac{ne^2\tau}{m}, \tag{2.8}$$

where n is the total number of electrons per unit of volume, then it is strictly connected to the density of states through the following integral:

$$n = \int_0^{E_F} N(\varepsilon)d\varepsilon. \tag{2.9}$$

It follows, then, that variations in the density of states $N(\varepsilon)$ must reflect in variations in the conductivity of the metal. Clearly, the presence of Cooper

pairs, dramatically affects the electronic spectrum. It is known, indeed, that in the superconducting phase they give rise to an energy gap in the density of states. Above the transition, if fluctuating Cooper pairs survive for a typical lifetime τ_{GL}, they will not only increase the conductivity via A-L processes, but they will also reduce it by affecting the DOS. Electrons bound into a pair, in fact, cannot partecipate to the current transport in the electron-channel.

If we imagine to have n_C fluctuating Cooper pairs in the normal state per unit volume, then the difference in the total carrier density will be $\Delta n_e = 2n_C$, yielding a correction to the conductivity given by the expression of equation 2.10:

$$\delta\sigma_{DOS} = -\frac{\Delta n_e e^2 \tau}{m} = -\frac{2n_C e^2 \tau}{m}. \tag{2.10}$$

Clearly, as mentioned above, this correction has a negative sign, as Cooper pairs reduce the total number of electronic carriers.

It is possible to evaluate the total concentration of fluctuating pairs at a temperature $T > T_c$ and then obtain the reduced temperature dependence of the DOS correction to conductivity: $\delta\sigma_{DOS} \propto log(\frac{1}{\sqrt{\epsilon}})$.

Comparing this result with the ones of eq.2.6, it clearly appears how the DOS related effects are much less singular in ϵ. In typical cases, thus, DOS effects are not able to overcome paraconductivity, the overall result, then, is the observed decreasing of the normal metal resistance before the transition temperature.

Maki-Thompson effect The effect studied by Maki [28] and a little later by Thompson [29], known as Maki-Thompson, is of purely quantum nature. It affects only transport coefficients and has a singular behaviour in principle similar to the paraconductivity one.

Electrons with nearly equal and opposite momenta interacting above T_c through the Cooper interaction, substantially modify the mean free path of their diffusive motion. As $T \to T_c$, the Cooper interaction dramatically increase:

$$g_{eff} = \frac{g}{1 - \nu g log(\frac{\omega_D}{2\pi T})} = \frac{1}{log(\frac{T}{T_c})} = \frac{1}{\epsilon} \tag{2.11}$$

This growth is due to a sort of resonant scattering, caused by the beginning of pairs' formation.

The Maki-Thompson effect is generated by a coherent scattering of electrons bound in Cooper pairs with the same impurity. Their initial distance will thus be the dimension of the Cooper pair, i.e. the coherence length $\xi(T)$. Nevertheless, in order to interact, the electrons must approach at a distance of order $\lambda_F = 1/k_F$.

Since the length covered by a diffusing electron is $R(t) \sim \sqrt{Dt}$, the scattering probability, evaluated in the weak-localization framework, will be identified with the self-interacting trajectories contribution (see [4], pages 135-136):

$$W \sim \int_{t_{min}}^{t_{max}} \frac{\lambda_F^{\mathcal{D}-1}}{R^{\mathcal{D}}(t)} v_F dt \tag{2.12}$$

The lower limit of integration t_{min} is determined by the time at which $R(t_{min}) \sim \xi(T)$, since this condition is necessary in order to let the electrons interact through Cooper interaction. The upper integration bound is, instead,

exstimated by the phase-breaking time τ_ϕ, since when coherence between electrons is lost, they can't bind together into Cooper pairs.

The total M-T correction $\delta\sigma_{M-T}$ is thus given by the product of the scattering probability times the effective interaction magnitude: $\delta\sigma_{MT}/\sigma = Wg_{eff}$. This value can be obtained through micropic considerations and it gives, in the $2\mathcal{D}$ case:

$$\delta\sigma_{MT} \sim \frac{e^2}{8\epsilon} log(\frac{D\tau_\phi}{\xi^2(T)}) \tag{2.13}$$

It is worth mentioning that the original work by Maki highlighted a dramatic divergence in the two-dimensional contribution, but it was later observed by Thompson that this infared divergence is indeed cut off by scattering on paramagnetic impurities, within a typical time τ_s, which destroys phase coherence. It is nowadays well known that phase breaking can be caused by many sources, such as paramagnetic defects, phonons, fluctuations and many others. This is the reason why the Maki-Thompson effect, even if expected to have a significant role, is often a non-leading term in contributions to extra conductivity in superconductors.

2.3 Effects on the Density of States

The object of this section will be the study of the change in the electronic density of states due to the persistence of Cooper pairs above the transition. As previously mentioned, this is a well-known phenomenon, called *pseudogap*, observed in several types of non-ordinary superconducting materials.

Because of the presence of fluctuating Cooper pairs, the number of free electronic states available for each particle decreases, thus giving rise to a decrease in the DOS. This feature is typically measurable in a range of temperatures depending both on the dimensionality of the sample and on the presence of impurities.

In order to account for the density of states in many body systems, the Lehmann representation of Green functions at finite temperature is an excellent tool. It gives a relation between the spectral density and the imaginary part of the retarded Green function describing the interacting particles.

For the sake of completeness, we report here this relation:

$$N(\omega) = -\frac{1}{\pi}\Im \int \frac{d^{\mathcal{D}}k}{(2\pi)^{\mathcal{D}}} G^R(\vec{k},\omega). \tag{2.14}$$

We remind that the retarded Green function is analytical in the complex upper-half plane. The solution of equation 2.14 in a superconductor with fluctuations was firstly derived by Abrahams, Redi and Woo [1] in 1970. The authors solved the problem in the presence of magnetic field and of impurities, highlighting the differences between the various dimensionalities. The energy dependence of the DOS indeed changes substantially modifying the dimensionality of the sample studied.

Calculations in the clean and dirty superconductor follow distinct paths. The presence of disorder makes some approximations legitimate, while its absence on the contrary forbits them, thus necessarily leading to different results, even if the general behaviour is similar throughout the variety of the systems.

The final results here reported are all obtained from eq.2.14, where the Green function is obtained through diagrammatic perturbation expansion, including fluctuations' contribution.

For a three-dimensional clean and isotropic sample one finds the contribution to the DOS from fluctuating Cooper pairs to be:

$$\frac{\delta N_{3,c}(\omega)}{N_{3,c}(\omega)} = -\frac{(4\pi)^{3/2}}{7\zeta(3)}\sqrt{Gi_{3,c}}\Re\Big[\frac{1}{\tau_{GL}^{-1} - \imath\omega + \sqrt{\tau_{GL}^{-1}(\tau_{GL}^{-1} - 2\imath\omega + \chi_3^2 T_c)}} \times \frac{\sqrt{T_c}}{\sqrt{\tau_{GL}^{-1} - 2\imath\omega + \chi_3^2 T_c}}\Big], \tag{2.15}$$

where $Gi_{3,c}$ is the Ginzburg-Levanyuk number ([60],[19]), defined as the reduced temperature at which the fluctuation correction to the heat capacity jump approaches the standard ΔC value, in some sense measuring the importance of fluctuations in the system. For a $3\mathcal{D}$ clean superconductor, this value reads:

$$Gi_{3,c} = 80\big(\frac{T_c}{E_F}\big)^4. \tag{2.16}$$

Since typically in bulk superconductors the transition temperature is many times smaller than the Fermi energy, we expect in these samples to see a very little fluctuation effect in the DOS.

Here $\chi_{\mathcal{D}}$ is a coefficient accounting for the different dimensionality: $\chi_{\mathcal{D}} = \pi\sqrt{\pi\mathcal{D}/7\zeta(3)}$. Finally, $\zeta(n)$ is the Riemann zeta function, $\zeta(3) \approx 1.202$.

For the clean two-dimensional metal, instead, the correction to the density of states, normalized to the normal value $N(\omega)$, is expressed in eq.2.17.

$$\frac{\delta N_{2,c}(\omega)}{N_{2,c}(\omega)} = -\frac{(4\pi)^2}{7\zeta(3)} Gi_{2,c}\frac{T_c^2}{\omega^2 + \chi_2^2 T_c\tau_{GL}^{-1}}\Big[1 - \frac{\omega}{\sqrt{\omega^2 + \chi_2^2 T_c\tau_{GL}^{-1}}} log\frac{\omega + \sqrt{\omega^2 + \chi_2^2 T_c\tau_{GL}^{-1}}}{\chi_2\sqrt{T_c\tau_{GL}^{-1}}}\Big]. \tag{2.17}$$

The general trend is similar to the one observed in three dimensions, showing a dip at the Fermi energy, taken as the zero point of the energy scale. This decreasing in the DOS increases as the temperature is lowered towards the transition temperature restoring the total energy gap at $T < T_c$. With increasing energy, the contribution from fluctuations reaches zero at some frequency value $\omega_0(T)$. Afterwards, the DOS shows a maximum at a frequency $\omega \sim \tau_{GL}^{-1}$, which is a precursor effect, anticipating the coherence peaks which will appear in the superconducting phase.

At larger energies, then, the normal value is restored, as expected since at such high energies Cooper pairs do not have enough binding energy to remain bound. As it is clear from eq.2.17 taking $\omega \gg \tau_{GL}^{-1}$, the fluctuation contribution to the DOS approaches zero as $log(\omega)\omega^{-2}$.

While evaluating dirty superconductor, scattering by impurities must be taken into account. As said above, This yelds results quantitatively different from the clean limit.

The dependence of the depth of the dip at $\omega = 0$ on the reduced temperature ϵ is indeed different in the two limits. For the clean superconductor, setting zero frequency, we obtain:

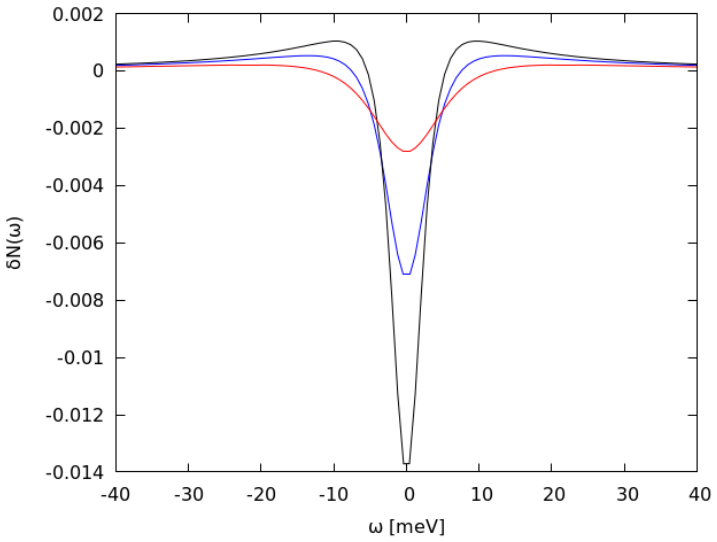

Figure 2.2: *The fluctuation contribution to the DOS for different temperatures in the 2$\mathcal{D}$ clean case. The black curve is evaluated at higher temperatures, and gives a correction to the DOS of roughly* 1.%. *Increasing the temperature (red curve) the contribution reduces to a* 0.1%.

$$\frac{\delta N_c(\epsilon)}{N_c} \sim -\begin{cases} \sqrt{Gi_{3,c}}\epsilon^{-1/2} & \mathcal{D}=3 \\ Gi_{2,c}\epsilon^{-1} & \mathcal{D}=2 \end{cases}, \tag{2.18}$$

while in the opposite limit of a dirty system, the ϵ dependence is:

$$\frac{\delta N_d(\epsilon)}{N_d} \sim -\begin{cases} \sqrt{Gi_{3,d}}\epsilon^{-3/2} & \mathcal{D}=3 \\ Gi_{2,d}\epsilon^{-2} & \mathcal{D}=2 \end{cases}, \tag{2.19}$$

showing, then, a stronger divergence at the transition $\epsilon \to 0$. At high energies, once again, the DOS recovers its normal value, since the fluctuation contribution vanishes as $\omega^{-3/2}$ for the three-dimensional system and as $\omega^{-}2$ in the two-dimensional case.

Another difference between the two limits arises in the evaluation of the energy scales relevant for the DOS, connected with the mechanism driving electronic motion in both cases. The energy scale at which the electronic spectrum firstly reaches its normal value, i.e. when $\delta N(\omega_0) = 0$, is indeed quantitatively different in dirty and clean superconductors.

For the former, this energy coincides with the inverse of the time necessary for the electrons to move apart on a distance $\sim \xi(T)$, as for lengthscales larger than the coherence lenght, no fluctuating Cooper pairs can survive. This inverse relaxation time is: $t_\xi^{-1} = D\xi^{-2}(T) \sim \tau_{GL}^{-1} \sim (T - T_c)$. In the latter, electrons move in a ballistic way, since impurity concentration is very low, changing the characteristic relaxation time and thus the energy scale: $t_\xi^{-1} \sim v_F\xi^{-1}(T) \sim \sqrt{T_c\tau_{GL}^{-1}} \sim \sqrt{T_c(T - T_c)}$.

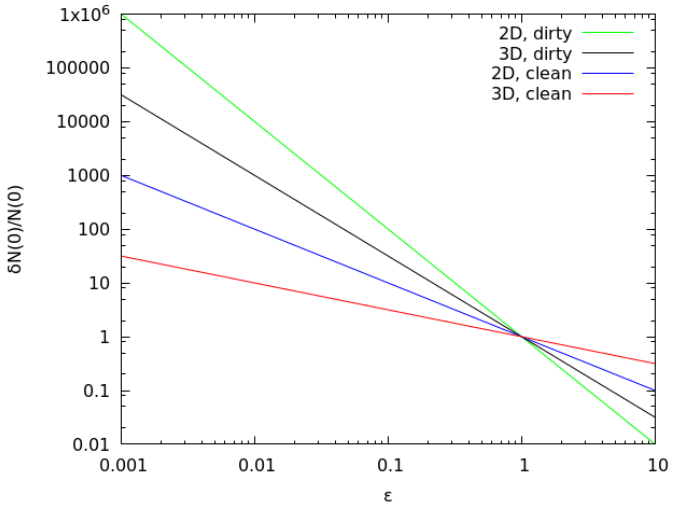

Figure 2.3: *Comparison of the behaviours in the different cases in a log-log scale. As in figure 2.1, at $\epsilon < 1$ we observe the faster divergence of the DOS in dirty superconductors and, both in the clean and in the dirty case, that two-dimensional systems always have a larger correction.*

Finally, an important check on the formulae hereby presented is possible, i. e. that the integral of the fluctuation contribution to the DOS over the entire positive energy range exactly vanishes:

$$\int_0^\infty \delta N(\omega) d\omega = 0. \tag{2.20}$$

We expect equation 2.20 to be fulfilled in such an electronic system, as the total number of particles must be conserved. This is indeed directly connected with the number of cells in the crystal, that cannot be changed by the interaction generating the fluctuating Cooper pairs. Thus, the only effect we must expect is a redistribution of the energy levels in a range around the Fermi energy, where the attractive interplay between electrons is effective.

Chapter 3

Fluctuations with anomalous diffusion law

3.1 Paraconductivity

As seen in Chapter 1, in the proximity of the transition temperature T_c, NbN ultra-thin films display an interesting phenomenon. In fact, although via Aslamazov-Larkin theory a $\frac{1}{\epsilon}$ behaviour is expected for paraconductivity in 2D systems, where $\epsilon \approx (T - T_c)/T_c$ (see eq. 2.6), experiments in NbN films are in contrast with the prediction, showing a ϵ^{-2} trend for a very extended range of temperatures. This is the expected result of the A-L theory for $\mathcal{D} \to 0$, as we shall show in a few steps, and should not be observed in the films under investigation, as they are two dimensional by all means.

The general expression for the paraconductivity in $\mathcal{D}$ dimensions, from which eq.2.6 is deduced, is:

$$\delta\sigma_{\mathcal{D}}(\epsilon) = \frac{\pi e^2}{4} \int \frac{d^{\mathcal{D}}q}{(2\pi)^{\mathcal{D}}} \frac{1}{\mathcal{D}} (\vec{\nabla}_q \nu_q)^2 \frac{1}{(\epsilon + \nu_q)^3}. \tag{3.1}$$

Since $\nu_q = \xi_0^2 |q|^2$, the whole integrand function depends only on $|\vec{q}|$ and the angular integration can be easily carried out.

$$\delta\sigma_{\mathcal{D}}(\epsilon) = \frac{\pi e^2 \Omega_{\mathcal{D}}}{4\mathcal{D}(2\pi)^{\mathcal{D}}} \int_0^{+\infty} dq (\frac{d\nu_q}{dq})^2 \frac{q^{\mathcal{D}-1}}{(\epsilon + \nu_q)^3} \tag{3.2}$$

Here $\Omega_D = \frac{2\pi^{\mathcal{D}/2}}{\Gamma(\frac{\mathcal{D}}{2})}$ is the surface of the unitary sphere in $\mathcal{D}$ dimensions (while $\Gamma(x)$ is the Euler gamma function). When $\mathcal{D} \to 0$, $\Gamma(\frac{\mathcal{D}}{2}) \sim \frac{2}{\mathcal{D}}$, so that the limit exists, and the expression for the paraconductivity becomes:

$$\delta\sigma_{\mathcal{D}\to 0}(\epsilon) = \pi e^2 \xi_0^4 \int_0^{+\infty} dq \frac{q}{(\epsilon + \xi_0^2 q^2)^3} \tag{3.3}$$

Changing the variable of integration from q to $t = \xi_0^2 q^2$ the expression for $\delta\sigma_{\mathcal{D}\to 0}$ becomes:

$$\delta\sigma_{\mathcal{D}\to 0}(\epsilon) = \frac{\pi e^2 \xi_0^2}{2} \int_0^{+\infty} dt \frac{1}{(\epsilon + t)^3} \tag{3.4}$$

and can be easily solved, leading to the $0\mathcal{D}$ formula for $\delta\sigma$

$$\delta\sigma_{\mathcal{D}\to 0}(\epsilon) = \frac{\pi\xi_0^2 e^2}{4\epsilon^2}. \tag{3.5}$$

This result shows that the limit for $0\mathcal{D}$ Aslamazov-Larkin paraconductivity exists, and has an ϵ dependence which is of the same type of the one observed in NbN films. However the quantity measured is not the bare paraconductivity, but the film paraconductance per square. This means that we have to divide the paraconductivity by a suitable length scale l, squared, in order to obtain a physical quantity comparable with experimental data.

$$\delta\sigma_{mes} = \frac{\pi e^2}{4\epsilon^2}\left(\frac{\xi_0}{l}\right)^2 \tag{3.6}$$

Unfortunately the *classical* A-L theory does not provide a value for l. Furthermore we know that, even though we might consider the supergrains composing the film as zero dimensional, in some sense, the system is indeed two dimensional and the grains are connected. We would then like to develop a theory which can account both for the length scale here absent and for the $0\mathcal{D}-2\mathcal{D}$ cross-over we expect. We in fact guess that there exist roughly two temperature ranges, one where fluctuations remain weakly confined in the supergrains, driving the system to its zero-dimensional like behaviour, closer to the transition, instead, the intergrains dynamics is leading, restoring the two-dimensional behaviour. Furthermore another issue intricates the problem. Cooper pairs with $\xi(T) < L_i$, the ones we argue are responsible of the $0\mathcal{D}$-like paraconductivity, indeed should have a three-dimensional behaviour. Since their dimension is smaller than the supergrain's size, then they should not interact with its border and consequently they should not feel the spatial constraint. This makes the interpretation of this anomalous feature particularly intricate.

In the following, we suggest a possible mechanism explaining the dynamics of fluctuations in this regime.

Looking to eq.3.1, we see that a more general form can be obtained with the introduction of a suitably weighted *square current density*, for the Cooper pair fluctuations:

$$N_{\mathcal{D}}(\nu) \equiv \int \frac{d^{\mathcal{D}}q}{(2\pi)^{\mathcal{D}}}(\vec{\nabla}_q\nu_q)^2\delta(\nu-\nu_q). \tag{3.7}$$

It is thus possible to write:

$$\delta\sigma_{\mathcal{D}} = \frac{\pi e^2}{4\mathcal{D}}\int_0^{+\infty} d\nu \frac{N(\nu)}{(\epsilon+\nu)^3} \tag{3.8}$$

and the standard A-L result is recovered with $N(\nu) = \frac{2\xi_0^{2-\mathcal{D}}\Omega_{\mathcal{D}}}{(2\pi)^{\mathcal{D}}}\nu^{\frac{\mathcal{D}}{2}}$. If we want to reproduce the observed $0\mathcal{D}-2\mathcal{D}$ cross-over, though, a different density function must be introduced.

In the system under examination we can put $\mathcal{D}=2$, and $N_2(\nu) = \frac{\nu}{\pi}$ is the correct density to recover the $2\mathcal{D}$ Aslamazov-Larkin behaviour for the paraconductivity. Herafter, instead of the bare ν dependence, we replace ν appearing in the expression for $N(\nu)$ with a function $g(\nu)$ defined as

$$g(\nu) \equiv \begin{cases} \nu & \text{if } \nu \leq \bar{\nu} \\ \bar{\nu} & \text{if } \nu > \bar{\nu}, \end{cases} \tag{3.9}$$

where $\bar{\nu}$ is a suitable constant.

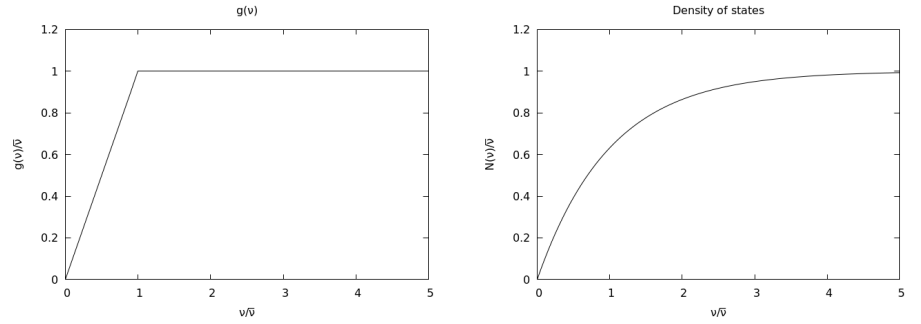

(a) *The function $g(\nu)$.*

(b) *Square current density calculated through the new dispersion law.*

Figure 3.1: *Comparison between $g(\nu)$ (a) and the square current density obtained with the anomalous ν_q (b): it is clear that the latter has a smooth cross over, while in the first it is discontinuous.*

With this new square current density, the paraconductivity is:

$$\delta\sigma_{\mathcal{D}=2}(\epsilon) = \frac{e^2}{8}\int_0^{+\infty} d\nu \frac{g(\nu)}{(\epsilon+\nu)^3} = \frac{e^2}{8}\Big[\int_0^{\bar{\nu}} d\nu \frac{\nu}{(\epsilon+\nu)^3} + \bar{\nu}\int_{\bar{\nu}}^{+\infty} d\nu \frac{1}{(\epsilon+\nu)^3}\Big], \tag{3.10}$$

and we obtain the cross over from one regime to the other, depending on the ϵ value,

$$\delta\sigma(\epsilon) = \frac{e^2}{16}\frac{\bar{\nu}}{\epsilon(\epsilon+\bar{\nu})}. \tag{3.11}$$

When $\epsilon \ll \bar{\nu}$ the standard $2\mathcal{D}$ behaviour is recovered, while when $\epsilon \gg \bar{\nu}$ a $0\mathcal{D}$-like trend is obtained:

$$\delta\sigma(\epsilon) = \frac{e^2\bar{\nu}}{16\epsilon^2}. \tag{3.12}$$

Since $\epsilon \approx \xi_0^2/\xi^2$ we can evaluate the temperature $\bar{T}$ at which the cross over takes place: $\xi(\bar{T}) \approx \xi_0\sqrt{\bar{\nu}}$. Comparison with the previously obtained $0\mathcal{D}$ limit of the standard A-L paraconductivity, eq.3.6, establishes a relation between $\bar{\nu}$ and the length scale l: $\bar{\nu} \approx 4\pi\big(\frac{\xi_0}{l}\big)^2$. The hypothesis of a non-trivial $g(\nu)$ dependence of the square current density solved the issues highlighted before in this section: an expression for the lengthscale l naturally appears, relating to the still unknown constant $\bar{\nu}$ and the cross over from one regime to the other is achieved at $\epsilon \approx \bar{\nu}$.

In order to continue, we must give this cross over function $g(\nu)$ a physical meaning. Nonetheless, we would like it to have a less abrupt discontinuity, as

we expect the cross over to be a continuous physical phenomenon. One possible explanation is that the dispersion law ν_q modifies, because of some still unknown mechanism, changing its behaviour above a typical momentum scale $\bar{q}$. Indeed, if we take as a dispersion law $\nu_q = \bar{\nu} log(1 + \frac{q^2}{\bar{q}^2})$ instead of $\nu_q = \xi_0^2 q^2$, then the square current density is, according to eq.3.7, $N(\nu) = \frac{\bar{\nu}}{\pi}(1 - e^{-\nu/\bar{\nu}})$. This is, as seen in fig.3.1, a smoothened version of the previous $g(\nu)$, making the cross over smeared in the range $\nu \in [1, 2]$, while for large ν the function is practically a constant.

It is now worth to have a deeper look at the diffusion law and its role. Since fluctuations in this superconductors move in a diffusive way, they must satisfy the diffusion equation:

$$\frac{\partial}{\partial t}\rho(\vec{x}, t) - D\nabla^2\rho(\vec{x}, t) = 0, \tag{3.13}$$

where $\rho(\vec{x}, t)$ is the Cooper pairs' propagator. Applying the Fourier transform to eq.3.13 we obtain a simple algebraic relation, which gives:

$$\rho(\vec{q}, \omega) = \frac{1}{\imath\omega - Dq^2}. \tag{3.14}$$

From this latter equation we can observe that the diffusion law must be related to the inverse lifetime of the diffusing Cooper pair. This substantial equality between diffusion law and inverse fluctuation's lifetime is very useful and will be widely used in the following.

The anomalous dispersion law is presented in fig.3.2: on the x axis the momentum q is normalized with respect to $\bar{q}$, while on the y axis $\frac{\nu_q}{\bar{\nu}}$ values are shown.

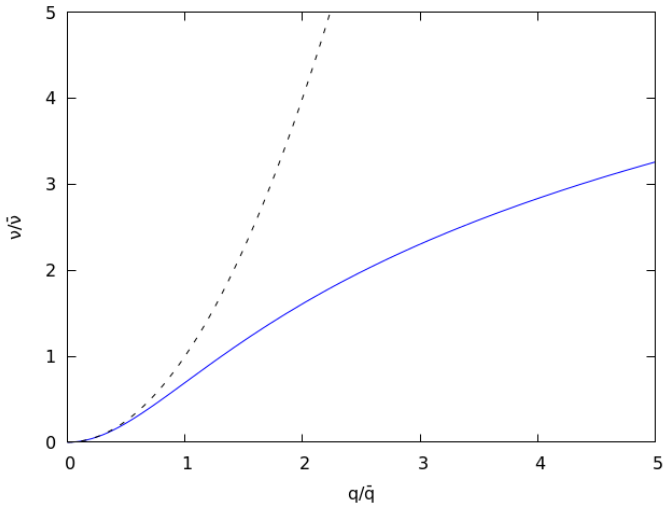

Figure 3.2: *The anomalous diffusion law ν_q, in blue, compared with the standard one (dashed). Clearly at small momenta the two diffusion laws are practically the same. When $q/\bar{q} > 1$, though, the anomalous diffusion is significantly lower than the standard one, thus increasing fluctuations' lifetime.*

While at small momenta, the normal behaviour $\nu_q \propto q^2$ is recovered, at wavevectors $q > \bar{q}$, instead, the logarithmic part is dominant, gving rise to a slow-down in the diffusion and consequently to an increase in the fluctuations lifetime. Physically, large wavelength fluctuations (with $\lambda \gg \frac{1}{\bar{q}}$) still obey the standard diffusion law, and thus give an essentially two-dimensional contribution, while small wavelength ones, with $\lambda \leq \frac{1}{\bar{q}}$, actually feel the logarithmic part of the anomalous ν_q, significantly increasing their lifetime and giving rise to a $0\mathcal{D}$-like behaviour. This phenomenological approach seems to explain the cross over observed in [2] as the result of an anomalous diffusion law, that leads to a slow-down of fluctuational Cooper pairs. The value of the wavevector $\bar{q}$ can be left as a free parameter and then obtained through the fitting with the data for the paraconductivity. Intriguingly, it was found that the best value is of the order of the inverse of the pseudogap inhomogenities regions $L_i \simeq 20 \div 50nm$. This gives a hint of what is really happening inside this strange superconductor: for some physical reason, whose nature is still to be clarified, the Cooper pairs seem to nearly *localize* in these regions, even if there is no strong and apparent morphological reason for them to do so. This localization, in grains of the typical dimension of $\frac{1}{\bar{q}}$, makes them have a longer lifetime. In turn, as we shall show in this thesis, this yelds a larger pseudogap in these regions. In fig.3.3 we can visualize what happens inside the NbN films: over small timescales and distancies the scattering inside each supergrain slows down the diffusion of fluctuations giving rise to the $0\mathcal{D}$-like behaviour (a). Over longer time and length scales, instead, the intragrain dynamics is recovered, restoring the usual $2\mathcal{D}$ behaviour (b). At these latter wave-vectors, anomalous and standard diffusion are indeed the same. Raising the temperature, we see from eq.3.11 that we approach the anomalous behaviour. This means that at higher temperatures the main contribution to paraconductivity comes from that momenta at which $\nu_q > \bar{\nu}$. Looking at the graph in figure 3.2, these wavevectors are the ones at which the standard diffusion law is way bigger than the anomalous one. Consequently, standard fluctuations have a much smaller lifetime than anomalous ones, thus the $0\mathcal{D}$-like regime is explained as the former are destroyed long before the latter.

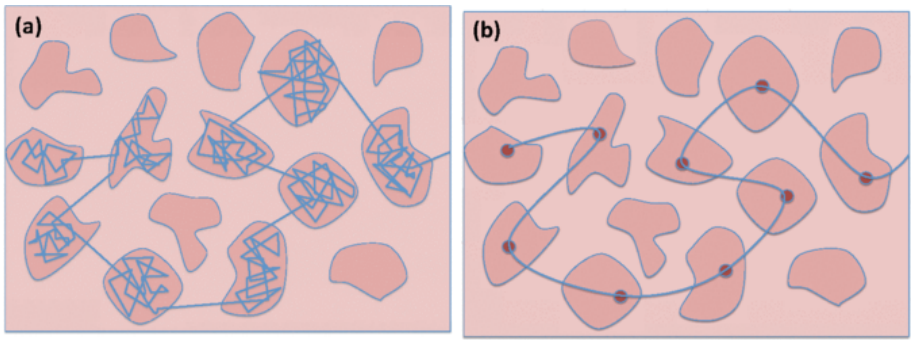

(a) *Scattering inside supergrains slows-down diffusion - 0D behaviour*

(b) *On longer lifetimes, intragrains dynamics restores 2D behaviour*

Figure 3.3: *Cooper pairs dynamics inside the NbN films on different timescales*

To proceed further with this hypothesis, agreement between DOS data, obtained through Scanning Tunnel Spectroscopy (STS), and the calculated density

of states, must be found.

3.2 Density of States

As discussed in the previous section, the proposed explanation of the anomalous paraconductivity behaviour of niobium nitride thin films could have a counterpart in the spectral electronic density of states. This seems to be suggested by the fact that the supergrains' dimension appears to be of the same order of the inverse of the best fit for the $\bar{q}$ parameter introduced in the modified diffusion law. As we shall see, the change in the diffusion law, certainly affects the density of states, too. We show, through this work, that the way the anomalous diffusion of fluctuating Cooper pairs influences the single electron DOS is in accordance with the trend measured in [2] and presented in section 1.3.1: our calculation indeed highilights an increase in the pseudogap in the anomalous $0\mathcal{D}$-like regime.

The next section is mainly dedicated to the mathematical details of the deduction of the DOS, the reader not interested in this matter, can directly move to equation 3.32 for the clean case and to eq.3.38 for the dirty one.

3.2.1 DOS calculation in the clean and dirty limit

According to quantum many body theory, as briefly mentioned in section 2.3, the single electron density of states of an interacting electronic system is computed through its retarded Green function: $N(\omega) = -\frac{1}{\pi}\int d^{\mathcal{D}}k \Im[G^R(\vec{k},\omega)]$. Introducing the spectral density of states $N(\vec{k},\omega)$ in a grand canonical ensamble, where $|\alpha\rangle$ and $|\alpha'\rangle$ are eigentsates of the hamiltonian $\hat{H}-\mu\hat{N}$, we have:

$$N(\vec{k},\omega) = \frac{1}{\mathcal{Z}}\sum_{\alpha,\alpha'}\delta(\omega_\alpha - \omega_{\alpha'} - \omega)|\langle\alpha|\psi_k^\dagger|\alpha'\rangle|^2(e^{-\frac{\omega_\alpha}{T}} + e^{-\frac{\omega_{\alpha'}}{T}}), \tag{3.15}$$

where $\mathcal{Z}$ is the partition function.

It follows that the retarded Green function $G^R(\vec{k},\omega)$ is:

$$G^R(\vec{k},\omega) = \int_{-\infty}^{+\infty}\frac{d\omega'}{2\pi}\frac{N(\vec{k},\omega')}{\omega'-\omega-\imath\eta}. \tag{3.16}$$

Through the Plemelij relation, since $\eta \to 0$, we can express the density of states as a function of the imaginary part of the retarded Green function, as stated above.

In chapter 2, we stressed that the prefactor of the paraconductivity in two-dimensional systems has an interesting universal value. This means that in superconducting films this factor, nominally $\hbar/16e^2$, is identical in the clean and in the dirty case. The theory exposed in sec.3.1, thus, did not assume none of the two distinct possibilities. This allowed us to evaluate the DOS with anomalous diffusion in both limits and compare it with its analogous in the standard diffusion case. The study, as we show in the next sections, proves how clearly the dirty superconductor displays the strongest pseudogap change, when anomalous diffusion is taken into account.

Clean superconductor To take into account the fluctuation contribution to the DOS in the clean limit, the diagramatic expression for $G(\vec{k},\omega)$ is:

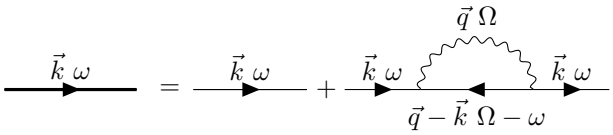

The total green function $G(\vec{k},\omega)$ (thick line) is, as shown in the diagram, the sum of a noninteracting part $G^0(\vec{k},\omega)=\frac{1}{i\omega-\xi_k}$ (simple line) and a self-energy contribution $\Sigma(\vec{k},\omega)$ connected through other two simple Green functions. Since in this paragraph we evaluate the clean case, we neglect the vertex corrections of the Green function. This corresponds to the limit $\tau\to\infty$, where τ is the relaxation time of the electronic motion.

In order to obtain the bare fluctuation contribution to the DOS normalized $\delta N(\omega)=\frac{N(\omega)-N_0}{N_0}$ it is enough to use the self-energy contribution, since $N_0=-\frac{1}{\pi}\int d^{\mathcal{D}}k\Im[G^0(\vec{k},\omega)]$. Working at $T>0$, Matsubara formalism is used, in which ω is a fermionic frequency ($\omega=2(n+1)\pi T$) and Ω is bosonic instead ($\Omega=2n\pi T$). We thus have, following the Feynman rules at finite temperature, to integrate over momenta $\vec{k}$ and $\vec{q}$ and to sum over Matsubara frequencies Ω:

$$\delta N(\omega)=-\frac{1}{N_0\pi}\int\frac{d^{\mathcal{D}}k}{(2\pi)^{\mathcal{D}}}\Im\Big[G_0^2(\vec{k},\omega)T\sum_{\Omega}\int\frac{d^{\mathcal{D}}q}{(2\pi)^{\mathcal{D}}}G_0(\vec{q}-\vec{k},\Omega-\omega)L(\vec{q},\Omega)\Big]. \tag{3.17}$$

$L(\vec{q},\Omega)$ is the fluctuation propagator (wavy line), obtained in a diagrammatic way in appendix A.1. We report here the final expression found in eq.A.10:

$$L(\vec{q},\Omega)=-\frac{1}{N}\frac{1}{\epsilon+\psi(\frac{1}{2}+\frac{|\Omega|}{4\pi T})-\psi(\frac{1}{2})-\frac{<(\vec{v}\cdot\vec{q})^2>_{F.S.}}{2(4\pi T)^2}\psi''(\frac{1}{2}+\frac{|\Omega|}{4\pi T})}. \tag{3.18}$$

The standard formulation interprets the prefactor of $\vec{q}^2$ as the diffusion coefficient of the theory, and expanding the digamma, $\psi(z)$, and tetra-gamma, $\psi''(z)$, functions, one obtains for the propagator, in the limit of $|\Omega|\ll T$, the following expression.

$$L(\vec{q},\Omega)\simeq-\frac{8T}{N_0\pi}\frac{1}{\tau_{GL}^{-1}+Dq^2+|\Omega|}, \tag{3.19}$$

where $\tau_{GL}^{-1}=\frac{8}{\pi}(T-T_c)$ is the inverse of Ginzburg-Landau relaxation time. In the case under investigation, we will substitute the standard diffusion law $\nu_q=\xi_0^2q^2$, with the one obtained in section 3.1, where now $\bar{\nu}\equiv D\bar{q}^2$, with D a suitable diffusion coefficient, which will be discussed later. With this replacement, the new expression for the fluctuation propagator in a two-dimensional system with supergrains is obtained.

$$L(\vec{q},\Omega)\simeq-\frac{8T}{N_0\pi}\frac{1}{\tau_{GL}^{-1}+D\bar{q}^2log(1+\frac{q^2}{\bar{q}^2})+|\Omega|} \tag{3.20}$$

The wave-vector $\vec{q}$ is clearly the momentum of the fluctuating Cooper pair, and thus must have a small value, as we know from BCS theory that Cooper

pairs have $\vec{q} \sim 0$. For small values of $\vec{q}$, quadratic terms in this momentum can be neglected leading to the approximation: $G_0(\vec{q}-\vec{k}, \Omega-\omega) \simeq \frac{1}{\imath(\Omega-\omega)-\xi_k+v_F\vec{\cdot}\vec{q}}$, where the Fermi velocity is taken legitimately as the electrons partecipating in the formation of Cooper pairs have wave-vectors in a small shell around the Fermi momentum. Since now everything depends only on the band ξ_k, it is possible to replace $\int \frac{d^d k}{(2\pi)^d}$ with an integral over the energy band: $\int_{-w_1}^{w_2} d\xi N(\xi)$. As we are far from any Van Hove singularity, taking the *normal* density of states as a constant N_0 is legitimate at this step. Moreover the energy scale typical of the gap in superconductors is of order $\approx 10 \div 100 \mu eV$, many times smaller than the total bandwidth $w_2 + w_1 \approx 1eV$; this means that setting the limits of the integration to infinity is an acceptable approximation, due to the fast convergence of the integral in the ultraviolet limit. Using this approximations, we have found the following expression for the fluctuations' contribution to the DOS:

$$\delta N(\omega) = -\frac{1}{\pi N_0} \Im\Big[N_0 T \sum_{\Omega} \int \frac{d^{\mathcal{D}} q}{(2\pi)^{\mathcal{D}}} L(\vec{q}, \Omega) \int_{-\infty}^{+\infty} d\xi \frac{1}{(\imath\omega - \xi)^2} \frac{1}{\imath(\Omega-\omega) - \xi + v_F\vec{\cdot}\vec{q}} \Big]. \tag{3.21}$$

At this point we can use the analytical continuation of the function to the complex plane, in order to solve the $d\xi$ integral by means of the residue method in a straightforward way. The integrand has two poles: $\xi_1 = \imath\omega$ of multiplicty 2 and $\xi_2 = v_F\vec{\cdot}\vec{q} + \imath(\Omega - \omega)$, which is a simple pole. In order to have a non-vanishing result, the two poles must be in opposite halves of the complex plane; furthermore, for the sake of semplicity, we decide to solve the integral in the half of the complex plane in which the simple pole appears.

$$\delta N(\omega) = -\frac{1}{N_0 \pi} \Im\Big[N_0 2\pi\imath T \sum_{\Omega} \int \frac{d^d q}{(2\pi)^d} \frac{sign(\omega)\theta(\omega(\omega-\Omega))}{(\imath\Omega - 2\imath\omega + v_F\vec{\cdot}q)^2} L(\vec{q}, \Omega) \Big]. \tag{3.22}$$

Since we are interested in the retarded Green function, we will take in a few steps the limit in which $\imath\omega \to \omega + \imath\eta$, therefore it is possible to take, without loss of generality, $\omega > 0$. To solve the sum over bosonic Matsubara frequencies, we look for a function that has poles at $\imath\Omega_n = 2n\pi\imath T$ values. The complex function $\coth(\frac{z}{2T})$ is one of those, as shown in eq.3.23:

$$\frac{e^{\frac{z}{2T}} + e^{-\frac{z}{2T}}}{e^{\frac{z}{2T}} - e^{-\frac{z}{2T}}} \approx \frac{2T}{z - \imath\Omega_n} \tag{3.23}$$

and its residue is $2T$. Thus, the result of the sum in eq.3.22 is obtained integrating over the contour C, shown in fig.3.4, the function of complex variable z:

$$\coth(\frac{z}{2T}) L(\vec{q}, \pm\imath z) \frac{1}{(z - 2\imath\omega + v_F\vec{\cdot}\vec{q})^2} \tag{3.24}$$

The function in eq.3.24 has a branch cut along the $\Re(z)$ axis, because of the modulus of Ω in $L(\vec{q}, \Omega)$, thus it is not analytical. To avoid this issue, keeping in mind that the retarded propagator will be used in the next, it is necessary to shift the complex variable $z \to z + \imath\omega$; after that, the function is analytical

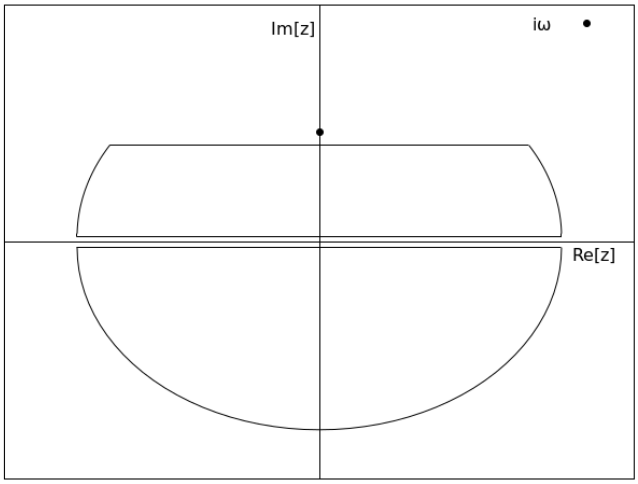

Figure 3.4: *The contour of integration in the complex plane*

on the lower half complex plane and $L(\vec{q},\Omega)$ can be replaced with its retarded counterpart. As a consequence its analytical continuation to $L^R(\vec{q},-\imath z)$ can now be performed without other problems and replacing $\imath\omega$ (where $\omega=(2n+1)\pi T$) with $\omega+\imath\eta$, where now ω is a real number and $\eta\to 0$, gives the expression for the retarded Green function. Since at $|z|\gg 1 \quad \coth(\frac{z}{2T})\simeq 1$, the whole integrand goes to 0 as $\frac{1}{|z|^3}$.

$$\begin{aligned}\Rightarrow \oint_c dz\coth(\frac{z+\omega}{2T})L^R(\vec{q},-i(z+\omega))\frac{1}{(z-\omega+\vec{v_F}\cdot\vec{q})^2}=\\ \int_{-\infty}^{+\infty} dz\coth(\frac{z+\omega}{2T})L^R(\vec{q},-i(z+\omega))\frac{1}{(z-\omega+\vec{v_F}\cdot\vec{q})^2}.\end{aligned} \tag{3.25}$$

Here, following [3] we have neglected a less singular part, coming from the shifting of the integration variable. With this substitution, equation 3.22 becomes:

$$\delta N(\omega)=-\frac{1}{N_0\pi}\Im\Big[\frac{N_0}{2}\int\frac{d^dq}{(2\pi)^d}\int_{-\infty}^{+\infty}dz\coth(\frac{z+\omega}{2T})L^R(\vec{q},-i(z+\omega))\frac{1}{(z-\omega+\vec{v_F}\cdot\vec{q})^2}\Big]. \tag{3.26}$$

To solve this integral, we adopt the so-called semi classical approximation, where $\coth(\frac{z}{2T})$ should be approximated with a simpler function; taking advantage of the fact that the main contribution to the integral comes from small values of $\frac{z+\omega}{2T}$, we replace $\coth(\frac{z+\omega}{2T})\approx\frac{2T}{z+\omega}$.

$$\Rightarrow\delta N(\omega)=-\frac{1}{N_0\pi}\Im\Big[N_0T\int\frac{d^dq}{(2\pi)^d}\int_{-\infty}^{+\infty}dz\frac{1}{z+\omega}L^R(\vec{q},-i(z+\omega))\frac{1}{(z-\omega+\vec{v_F}\cdot\vec{q})^2}\Big] \tag{3.27}$$

Inserting the expression of L^R from eq.3.19, we clearly see the presence of three poles in the complex plane: $z_1=-\omega-\imath(D\vec{q}^2 log(1+\frac{q^2}{\vec{q}^2})+\tau_{GL}^{-1})$, $z_2=-\omega$,

$z_3 = \omega - \vec{v_F} \cdot \vec{q}$. Since both z_2 and z_3 are real, and the contour of integration avoids the real axis, the only pole whose residue contributes to the integral is z_1. It is a simple pole and its residue is easily found.

$$\Rightarrow \delta N(\omega) = -\frac{16T^2}{N_0\pi}\int \frac{d^2q}{(2\pi)^2}\Re\Big[\frac{1}{(\vec{v_f}\cdot\vec{q} - 2\omega - \imath(\tau_{GL}^{-1} + D\bar{q}^2 log(1+\frac{q^2}{\bar{q}^2})))^2}$$
$$\times \frac{1}{(\tau_{GL}^{-1} + D\bar{q}^2 log(1+\frac{q^2}{\bar{q}^2}))}\Big] = -\frac{16T^2}{N_0\pi}\int_0^{q_{cut}} \frac{qdq}{(2\pi)^2}\frac{1}{(\tau_{GL}^{-1} + D\bar{q}^2 log(1+\frac{q^2}{\bar{q}^2}))}$$
$$\times \Re\int_0^{2\pi} d\theta\Big[\frac{1}{(v_f q cos(\theta) - 2\omega - \imath(\tau_{GL}^{-1} + D\bar{q}^2 log(1+\frac{q^2}{\bar{q}^2})))^2}\Big]. \tag{3.28}$$

Replacing $t = tg(\theta/2)$, $dt = (1 + tg^2(\theta/2))d\theta/2$, $d\theta = 2\frac{dt}{1+t^2}$, the angular integration can be solved analytically with the residue method,

$$\int_0^{2\pi} d\theta \frac{1}{(v_F q cos(\theta) - z)^2} = 4\int_0^{+\infty} \frac{dt}{1+t^2}\frac{1}{(v_F q\frac{1-t^2}{1+t^2} - z)^2}, \tag{3.29}$$

where $z = 2\omega + \imath(\tau_{GL}^{-1} + D\bar{q}^2 log(1+\frac{q^2}{\bar{q}^2}))$.

The integrand is even in t, hence we can extend the lower limit of integration to $-\infty$:$\int_0^{+\infty} f(t) = \frac{1}{2}\int_{-\infty}^{+\infty} f(t)$. Furthermore the function is analytical on the real axis and it can be analytically continued to the complex plane simply replacing t with $\zeta \in \mathbb{C}$. Now the integration is along a complex contour, which can be chosen arbitrarily within the ones that give the correct integral on the real axis.

$$2\int_{-\infty}^{+\infty} dt \frac{1+t^2}{(v_F q(1-t^2) - z(1+t^2))^2} = \frac{2}{(v_F q + z)^2}\oint_c d\zeta \frac{1+\zeta^2}{(\zeta - t_+)^2(\zeta - t_-)^2}. \tag{3.30}$$

Here $t_\pm = \pm\sqrt{\frac{v_F q - z}{v_F q + z}}$ are the poles of the complex function; since they are in opposite halves of the complex plane, we can choose either to close the contour c in the upper or in the lower half.

Recalling from eq.3.28 that we are interested only in the real part of the integral in eq.3.30, the final result is:

$$\Re\frac{2}{(v_F q + z)^2}\oint_c d\zeta \frac{1+\zeta^2}{(\zeta - t_+)^2(\zeta - t_-)^2} = \Im\frac{2\pi z}{(v_F^2 q^2 - z^2)^{3/2}}. \tag{3.31}$$

Once the integral in θ has been solved, a deeper insight at the features of the density of states is possible, since now the only integration in dq is left:

$$\delta N(\omega) = -\frac{32T^2}{\pi N_0}\int_0^{q_{cut}} \frac{qdq}{(2\pi)}\frac{1}{(\tau_{GL}^{-1} + D\bar{q}^2 log(1+\frac{q^2}{\bar{q}^2}))}$$
$$\times \Im\frac{2\omega + \imath(\tau_{GL}^{-1} + D\bar{q}^2 log(1+\frac{q^2}{\bar{q}^2}))}{(v_F^2 q^2 - (2\omega + \imath(\tau_{GL}^{-1} + D\bar{q}^2 log(1+\frac{q^2}{\bar{q}^2})))^2)^{3/2}}. \tag{3.32}$$

Dirty superconductor The main difference with respect to the clean limit, is the fact that a finite relaxation time τ is taken into account in the evaluation of the Green function of the dirty superconductor. This leads to a shift in the fermionic frequency $\omega \to \omega + sign(\omega)/2\tau$ and to a vertex correction in the Feynman's diagram. The vertex correction arises from the ladder summation of impurity's scattering. Since in the diagram presented in the previous paragraph there were two vertices, this contribution will apear as a squared quantity: $\Lambda^2(\vec{q}, \omega, \Omega)$.

$$\Lambda(\vec{q}, \omega, \Omega) = \frac{1}{\tau} \frac{1}{D\bar{q}^2 log(1 + \frac{q^2}{\bar{q}^2}) + |2\omega + \frac{sign(\omega)}{\tau} - \Omega|}. \tag{3.33}$$

With this changes, the equation for the fluctuations' contribution to the two-dimensional DOS becomes:

$$dN(\omega) = -\frac{T}{\pi N_0} \Im\Big[\sum_{\omega} \int \frac{d^2q}{(2\pi)^2} L(\vec{q}, \Omega)\Lambda^2(\vec{q}, \omega, \Omega) \int \frac{d^2k}{(2\pi)^2} G_0^2(\vec{k}, \omega) G_0(\vec{q}-\vec{k}, \Omega-\omega)\Big]. \tag{3.34}$$

Because of the presence of the vertex part, the main $\vec{q}$ dependence comes from the poles in Λ^2 and then an easier form for the free electron Green function in eq.3.34 can be used here, taking only the $\vec{q} = 0$ value of $\xi_{\vec{k}-\vec{q}}$.

In order to solve the d^2k integral, a strategy similar to the one presented in the previous paragraph (see eq.3.21) can be used. We therefore pass from a two-dimensional integration in d^2k to a monodimensional integral in $d\xi$ times the two-dimensional normal density of states N_0.

$$\int \frac{d^2k}{(2\pi)^2} \frac{1}{(\imath\omega - \xi_{\vec{k}})^2(\imath(\Omega - \omega) - \xi_{\vec{k}})} = N_0 \int_{-\infty}^{+\infty} d\xi \frac{1}{(\imath\omega - \xi)^2(\imath(\Omega - \omega) - \xi)}. \tag{3.35}$$

After the analytical continuation to the complex plane and the use of the residue theorem we obtain the result:

$$N_0 \int_{-\infty}^{+\infty} d\xi \frac{1}{(\imath\omega - \xi)^2(\imath(\Omega - \omega) - \xi)} = -\frac{2\pi\imath sign(\omega)\theta(\omega(\omega - \Omega))N_0}{(2\imath\omega - \imath\Omega)^2}. \tag{3.36}$$

The main difference with the clean case is clear here: we do not have any $\vec{v}_F \cdot \vec{q}$ term in eq.3.36.

Using this result and the explicit expressions for $L(\vec{q}, \Omega)$ (eq.3.20) and $\Lambda(\vec{q}, \omega, \Omega)$ (eq.3.33), we obtain for $\delta N(\omega)$ the following formula:

$$\delta N(\omega) = \frac{16T}{\pi N_0 \tau} \Re\Big[\int \frac{d^2q}{(2\pi)^2} T \sum_{\Omega} \frac{sign(\omega)\theta(\omega(\omega - \Omega))}{(2\imath\omega - \imath\Omega)^2 (D\bar{q}^2 log(1 + \frac{q^2}{\bar{q}^2}) + |2\omega - \Omega|)^2} \times \frac{1}{(\tau_{GL}^{-1} + D\bar{q}^2 log(1 + \frac{q^2}{\bar{q}^2}) + |\Omega|)}\Big]. \tag{3.37}$$

In order to solve the Matsubara sum in eq.3.37, we follow exactly the same steps of the clean case. Clearly the poles will be different here, but the main

stages of the calculation are identical: we again use $coth(z/2T)$ as auxiliary function, we then shift $z \to z + \imath\omega$, in order to obtain an analytical integrand and get rid of the moduli.

The final expression for the fluctuational DOS is then obtained observing that the angular part of the d^2q integration is trivial as nothing depends on θ.

$$\delta N(\omega) = -\frac{16T^2}{\pi N_0 \tau}\int_0^{q_{cut}} dq \frac{q(4(|\omega|+\frac{1}{2\tau})^2 - (\tau_{GL}^{-1} + D\bar{q}^2 log(1+\frac{q^2}{\bar{q}^2}))^2)}{(\tau_{GL}^{-1} + D\bar{q}^2 log(1+\frac{q^2}{\bar{q}^2}))(2D\bar{q}^2 log(1+\frac{q^2}{\bar{q}^2}) + \tau_{GL}^{-1})^2} \times \frac{1}{(4(|\omega|+\frac{1}{2\tau})^2 + (\tau_{GL}^{-1} + D\bar{q}^2 log(1+\frac{q^2}{\bar{q}^2}))^2)^2}. \tag{3.38}$$

At the end of this section, we remark that unfortunately solving the last integral is a hopeless effort both in the clean (eq.3.32) and in the dirty (eq.3.38) limit. Only numerical solutions are available, and thus we used a C++ environment in order to obtain the DOS curves presented in the next sections.

3.2.2 Comparison between anomalous and normal DOS curves

Now that we have obtained, for the first time, the expressions for the contribution of anomalous fluctuations to the DOS in the clean, eq.3.32, and in the dirty case, eq.3.38, we can compare them with the standard result. We look for an increase in the pseudogap, proving that anomalous diffusion can indeed give rise to electronic spectra inhomogeneities.

We expect this effect to be stronger at higher temperatures and smaller $\bar{q}$. In order to check this behaviour, we compared different curves obtained at different T/T_c ratios and at different L_i values.

Both in the clean and in the dirty limit, we kept all the other parameters fixed. As a momentum cut-off we took the limit of the Brillouin zone $1/a$, where $a = 0.44\ nm$ is the lattice constant. For the Fermi energy we chose $E_F = 300\ meV$, a typical order of magnitude in two-dimensional systems. The diffusion constant D was taken at its standard BCS value $D = 8T_c/\pi\xi_0^2$ and the normal two-dimensional DOS N_0 was $N_0 = mp_F/2\pi^2 L$, where L is the sample thickness.

Clean superconductor The curves obtained with anomalous diffusion in the clean limit displayed effectively an increase in the pseudogap with respect to the standard DOS. Nevertheless, as we will see in this paragraph, this effect is really small, compared to the one obtained in the dirty case, and probably cannot explain the experimental data obtained in [2].

As reported in figure 3.5 (a), anomalous diffusion can indeed give an increase in the pseudogap. All the curves display a decrease in $N(\omega)$ with respect to the normal DOS curve, the black line. At $\omega = 0$ all the data have the same value for all the different $\bar{q}$ studied and independently on the fact that anomalous or normal diffusion is taken into account.

Nevertheless, as ω increases the effect of a pseudogap enhancement becomes clear. We stress that the energy scale $\tilde{\omega}$ at which the normal DOS and the

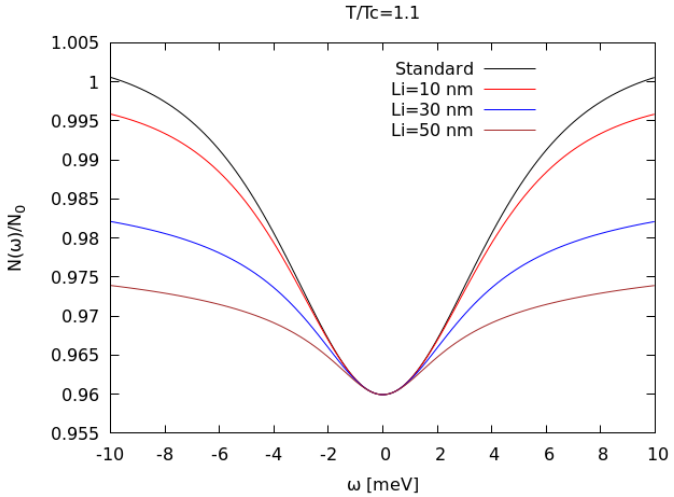

(a) *Comparison of the standard DOS (black line) with curves obtained with anomalous diffusion at different $\bar{q}$ values. $T/T_c = 1.1$. It is clear how increasing $L_i = 1/\bar{q}$ the effect on the pseudogap increases. It is also interesting to notice that $N(0)$ seems to be totally independent on the $\bar{q}$ choice*

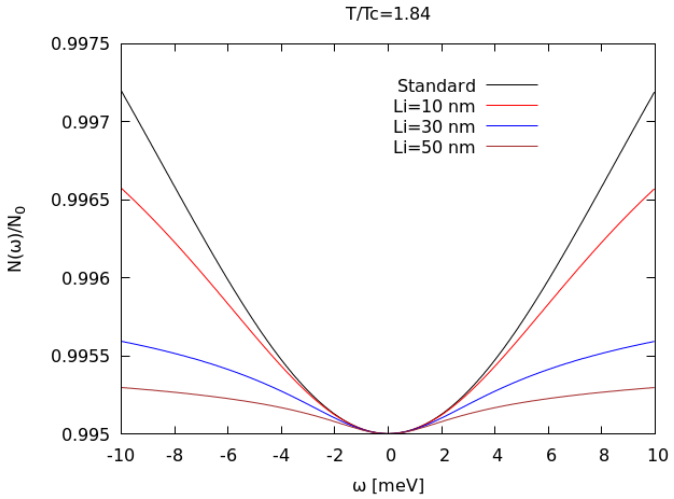

(b) *Comparison of the standard DOS (black line) with curves obtained with anomalous diffusion at different $\bar{q}$ values. $T/T_c = 1.84$. With respect to the data at a lower temperature, we notice that in this curves th effect seems to be stronger*

Figure 3.5: *Pseudogap at different supergrains' size and at different temperatures*

anomalous one begin to be different is strictly dependent on $\bar{q}$. From fig.3.5(a) it is possible to observe that the lower $\bar{q}$, i.e. the higher L_i, the lower this energy scale. There must, thus, be a direct dependence of $\tilde{\omega}$ on $\bar{q}$.

Studying the various energy scales present in eq.3.32, we obtained $\tilde{\omega} \propto v_F \bar{q}$.

At higher temperatures we expect the anomalous regime to be more effective

in reducing the density of states. In figure 3.5(b) we show DOS curves obtained at a T/T_c ratio of 1.84, thus far away from the transition.

Once again $N(0)$ is the same for all the curves shown in fig.3.5(b), proving that this behaviour is very strong with temperature. In this regime, we observe that the two curves with smaller $\bar{q}$ (the blue and the brown one) seem to reach a plateau at high frequencies, while the red curve ($L_i = 10\ nm$) and the black one grow up to unity.

In the clean limit, then, we noticed how certainly anomalous diffusion can be the cause of a pseudogap enhancement, giving a decrease in the density of states over a wide range of temperatures. Nevertheless, if we look for a quantitative result, comparable with the experiments, we must recognise that in the clean superconductor anomalous fluctuations are not such strong. We must stress that a particular behaviour, i.e. the fact that anomalous and standard diffusion give the same $N(0)$ value, is definitely against observations. As observed in section 1.3, and particularly in figure 1.21, we expect the effect of anomalous diffusion to be important at small frequencies.

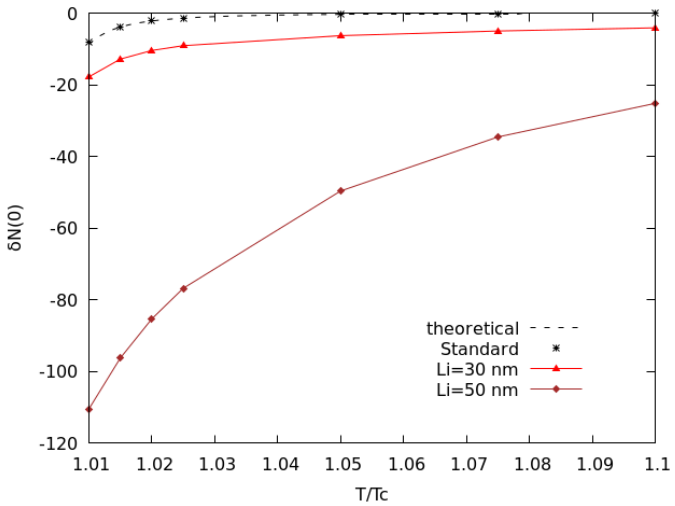

Figure 3.6: *$\delta N(0)$ values at different T/T_c ratios. Dashed line corresponds to the theoretical behaviour, red triangles to $L_i = 30\ nm$ and brown points to $L_i = 50\ nm$. It is possible to observe an enormous increase in $\delta N(0)$ with increasing L_i.*

Dirty superconductor In the dirty limit, the effect of the anomalous diffusion is definitely larger and stronger with temperature. This fact is easy to believe, as we indeed expect the dirty framework to be more correct to describe the NbN films, which are homogeneously disordered.

While in the clean limit the only adjustable parameters were temperture T and supergrains' size $L_i = 1/\bar{q}$, in the dirty case also the relaxation time τ can be set as a parameter, as we do not know its exact value for our samples.

As a first step we studied the curves' behaviour in $\omega = 0$, plotting $N(0)$ vs T/T_c. The theoretical behaviour, as reported in section 2.3, for this quantity in the normal diffusion regime is $N(0) \propto \epsilon^{-2}$.

In figure 3.6 we compare the theoretical curve with data obtained with different values of $\bar{q}$ in a range from 1000 to 1/50 nm^{-1}. The $\bar{q} = 1000\ nm^{-1}$ plot was made to check that at high $\bar{q}$ the anomalous diffusion gives the same results as the normal one. We notice that for increasing L_i the shape of the curve remains the same, but the values of $N(0)$ are definitely larger for increasing supergrains' size.The data in figure 3.6 highlight, in the dirty case, a strong dependence of the value of the DOS in $\omega = 0$ on $\bar{q}$.

This is an important difference with the clean limit, where $N(0)$ was the same in normal and anomalous diffusion. As already mentioned, this behaviour is similar to the one measured on NbN films and thus we expect the application of the dirty approach to anomalous diffusion to be the more correct.

Moreover, comparison of the DOS curves at $T/T_c = 1.1$ (fig.3.7(a)) and at $T/T_c = 1.84$ (fig.3.7(b)) show that the decrease in the DOS is always present.

All the curves presented in these two figures were obtained fixing the disorder strength at $1/\tau = 20\ meV$, many times smaller than the Fermi energy. We will see in the next lines that this parameter modifies the curves in an interesting way. In the first graph (fig.3.7(a)) the temperature is $T = 4.2\ K$, thus close to the transition temperature $T_c = 3.8\ K$. Here the effect of anomalous fluctuations is huge and its dependence on the $\bar{q}$ parameter is dramatic. Indeed, we notice that the blue curve, with $\bar{q} = 1/10\ nm^{-1}$ is pratically identical to the standard DOS (black line), while the red ($\bar{q} = 1/30\ nm^{-1}$) and the brown ($\bar{q} = 1/50\ nm^{-1}$) DOS have a much larger deviation.

In the second figure, DOS curves are evaluated at $T = 7\ K$, well inside the $0\mathcal{D}$-like regime of NbN films. Here the effect of the anomalous diffusion is quantitatively smaller, but it gives anyway a very strong pseudogap with increasing temperature. We observe that also the blue curve ($L_i = 10\ nm$), that at $T = 4.2\ K$ was very similar to the standard curve, at this higher temperature deviates significantly from it, giving rise to a persistent pseudogap.

At the end of this section we would like to stress the behaviour of DOS curves upon changing $1/\tau$. The precise value of the relaxation time is not known, and its variations can strongly modify our curves, particularly when compared with experiments. At the present stage, we suggest that this comparison could also give a good estimation of the disorder strength of the studied samples.

A generical behaviour is clear from the panel: increasing $1/\tau$ the effect of anomalous diffusion on the pseudogap increases. Therefore, we expect superconducting films with higher impurity concentration to have a larger pseudogap, which survives to higher temperature. This fact is in agreement with the experimentally observed strong pseudogap in granular superconductors.

In this section, then, we have observed how the comparison between anomalous and standard density of states results in a larger pseudogap for the former, both in the dirty and in the clean limit. This is certainly a good result, as we were looking for such an effect due to anomalous diffusion. Furthermore, comparing the curves obtained in the dirty and in the clean case, it appears that in the latter we obtain a much smaller effect, and on an energy range which is different from the one expected from experiments.

In figure 3.8, lastly, we compared anomalous DOS curve with different $1/\tau$ values at a temperature $T = 5\ K$ and chosing a fixed $L_i = 30\ nm$, showing how increasing the impurity concentration the effect of the anomalous diffusion is larger.

Therefore the anomalous diffusion of fluctuating Cooper pairs gives the cor-

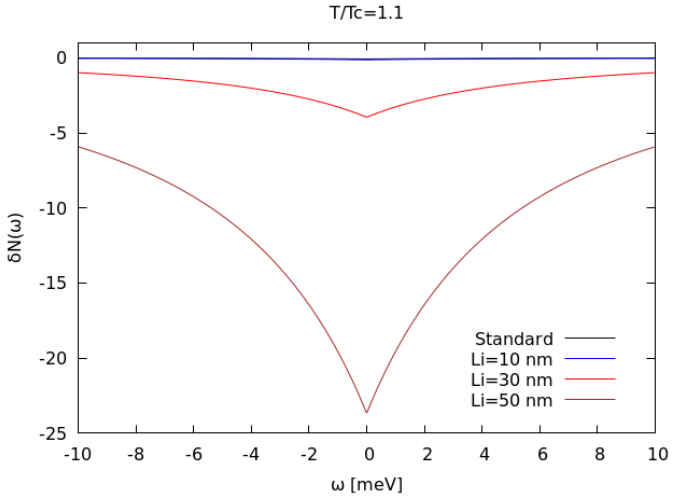

(a) *DOS curves compared at $T/T_c = 1.1$ for different L_i values. An enormous increase in the depth of the DOS is observed with increasing L_i. In this calculation $1/\tau = 20\ meV \sim 0.067\ E_F$*

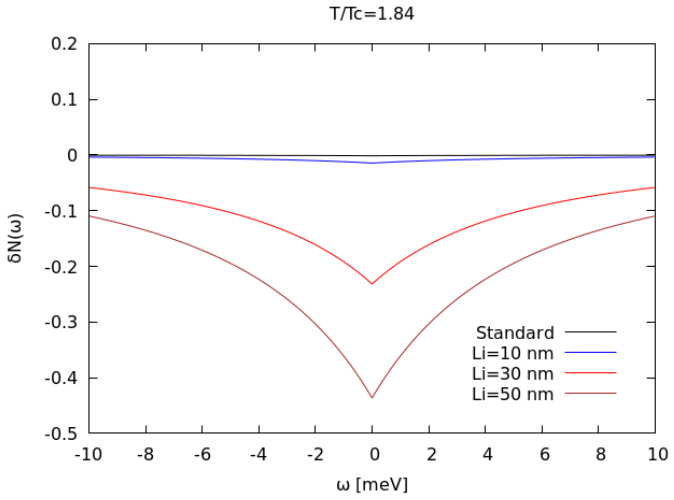

(b) *DOS curves for the same L_i values of panel (a) but at a different T/T_c ratio. We observe that at higher temperatures, the effect of the increase of the pseudogap is still large, but it has decreased*

Figure 3.7: *Pseudogap at different supergrains' size and at different temperatures*

rect DOS behaviour in the dirty two-dimensional superconductor case, which indeed seems to be the most adequate to describe NbN thin films.

In the following sections, then, we will discuss the fitting of anomalous DOS curves obtained in the dirty framework with experimental data from Carbillet et al. paper [2].

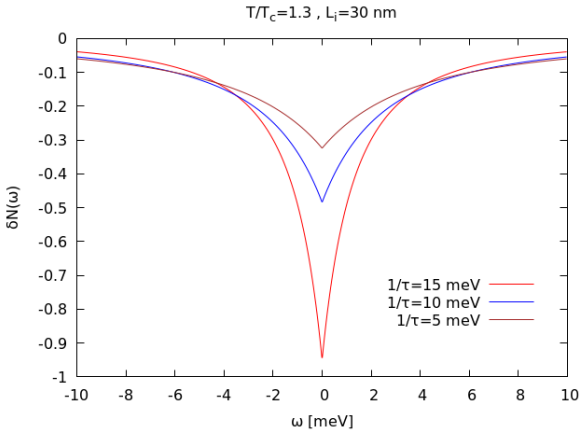

Figure 3.8: *Comparison of anomalous DOS curves at different $1/\tau$ values. It clearly appears that increasing the inverse disorder strength, the pseudogap decreases. This means that samples with more impurities, which have a lower τ, should have a larger pseudogap.*

3.3 Comparison with experiments

In this thesis, untill now, we have found that theoretical DOS curves obtained through anomalous diffusion effectively display a stronger pseudogap in two-dimensional films. Furthermore we proved that the best way to describe this increase in the pseudogap is the dirty superconductor framework. Using this approach, we found a huge enhancement of the depression of the DOS around the Fermi energy, dependent on various parameters. Among them, certainly the supergrains' size $L_i = \bar{q}^{-1}$ and the disorder strength $1/\tau$ are the most physically relevant. We would like to stress here that to these two physical quantities, at least one could be added as a parameter: the diffusion coefficient D. So far we took it in its standard value for the dirty superconductor. Nevertheless, since we argue that diffusion is strongly modified in these films, one could expect also the coefficient to be different from its normal value.

So far, we investigated anomalous diffusion under a mostly theoretical point of view, studying different cases and regimes. At this point, though, our aim is to compare our phenomenological predictions with experimental results. We will, thus, devote the rest of this thesis to the comparison with the DOS curves obtained on NbN thin films in [2].

In their paper, the authors measured electronic spectrum inhomogeneities over a lengthscale $L_i \sim 20 \div 50\ nm$ which is not related to any morphological relevant scale. At temperatures $T > T_c$ they measured an increasing of the pseudogap in these regions, as we can see from fig.3.9. In this panel, two different DOS curves referring to different regions are compared. The red curve was measured in a region of higher pseudogap.

This data were obtained for the thinner of the NbN samples ($t = 2.14\ nm$, $T_c = 3.8\ K$) at a temperature of $4.2\ K$. One can immediately notice that at small energies, $V \in [-1, 1]$, the red curve has a deeper dip in the DOS. However, with increasing energy the two curves substantially overlap.

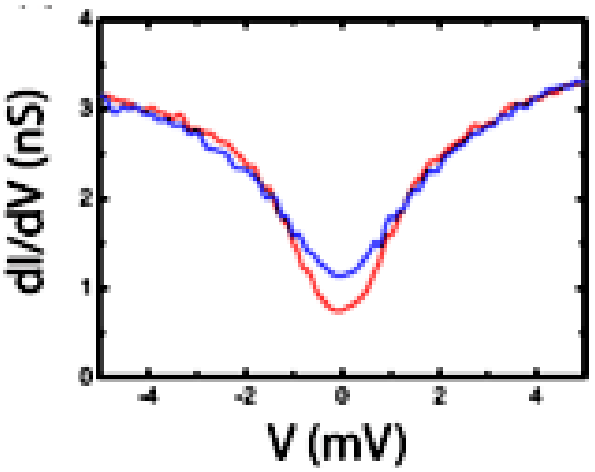

Figure 3.9: *Comparison of two different DOS curves, obtained on a NbN thin film (thickness $t = 2.14\ nm$). The red curve was measured in a high-pseudogap region, or supergrain, while the blue one has a smaller pseudogap. It is worth notice that the difference between the two curves is larger at small V values*

As previously said, we must compare our curves with these experiments. In order to achieve this result, we must adjust the experimental data to remove some effects we are not accounting for in our work. A generical suppression of the DOS is typically present in many electrons systems, the so-called Altshuler Aronov effect ([27]),which is essentially leading in DOS suppression at high temperatures. Since this phenomenon is out of our analysis, we decided to devide the experimental curves presented in figure 3.9 by some high temperature data, thus obtaining the curve used for comparison in the following figures. After this procedure, we adjusted the parameters of the expression in eq.3.38 to find a quantitative agreement between the experimental data and our theoretical prediction.

We know that the supergrains' size is $L_i \sim 20 \div 50\ nm$ and that the relaxation time τ must satisfie $1/\tau \ll E_F$. Moreover we observe that in their analysis on paraconductivity, the authors of [2], had to modify the standard Aslamazov-Larkin coefficient, in order to obtain a good fit. Consequently we expect a renormalization of our results of the same order of magnitude ($\sim 30\%$), when we compare them with experiments.

Firstly we looked for a quantitative agreement with experimental data, concerning the depth of the DOS fluctuative contribution. We investigated a range of disorder strengths varying from $1/\tau = 5meV$ to $1/\tau = 20meV$. For each of them, we calculated the DOS at different L_i values, fitting the results with the original curve.

In figure 3.10 we report the results of the calculation of the DOS at $T/T_c = 1.1$, $L_i = 16.5\ nm$ and $1/\tau = 5\ meV$. Quantitatively there is good agreement between the theoretical, red curve, and experimental, black crosses, data at small ω values. This behaviour has been observed at all the disorder strengths investigated, yielding, for each of them, a different $\bar{q} = L_i^{-1}$ value. All the different supergrains' sizes extracted from the fit are in reasonable agreement

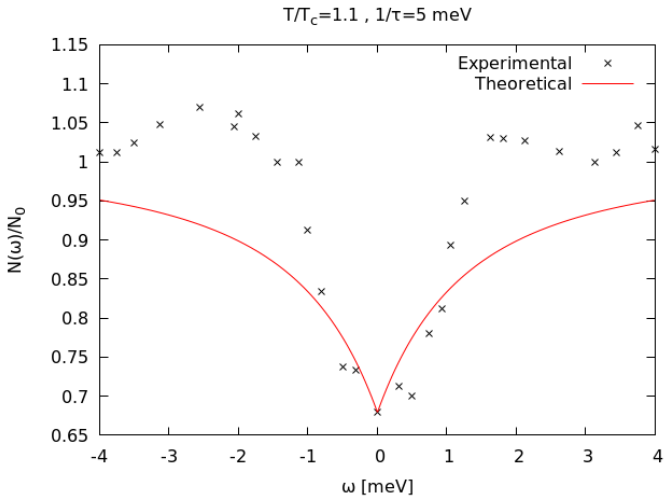

Figure 3.10: *Comparison of the data from Carbillet et al. ([2]), black crosses, with a DOS curve obtained with anomalous diffusion, red curve. Fitting parameters for this case are:* $L_i = 16.5\ nm$, $1/\tau = 5\ meV$.

with the estimated values reported in [2] both from morphological measurements and from paraconductivity fit. We can, then, observe from this result that the same phenomenological argument, i. e. the anomalous diffusion hypothesis, can explain both paraconductivity and electronic spectra strange behaviour of NbN ultra-thin films.

There is at leas one more interesting information that can be obtained from the quantitative comparison of theoretical curves with experimental data. It is, indeed, possible to plot L_i as a function of the disorder strength $1/\tau$, using the data obtained from the different fit. These data are shown in figure 3.11, where we can appreciate the almost linear increase of L_i with increasing $1/\tau$. Then it means that our phenomenological framework can give good results over a wide range of possible disorder strengths. In more detail, we found that at higher impurity concentrations (larger $1/\tau$) a larger supergrains' size gives the best fit.

Even if this is not a prove of a direct correlation between the two quantities, following our theoretical predictions we would expect a more disordered material to have larger supergrains. Unfortunately, at this stage, we do not have other samples with different impurity concentration to prove this prediction.

Even though the quantitative agreement between the fluctuative contribution to the DOS and the experimental results is good, a failure of the qualitative shape of the theoretical curve is evident, compared with the experiment. Especially around $\omega = 0$, we observe that the typical behaviour of the two curves is very different. In the experimental curve, the dip at $\omega = 0$ is rounded, while in our theoretical DOS it has a cusp-like trend. We are, thus, able to reproduce the quantitative correction, by adjusting the fitting parameters, but we cannot achieve qualitative agreement, at this stage.

We highilighted in section 1.3.2 that consistency between experimental paraconductivity data and anomalous diffusion theory is achieved only if we assume the critical temperature of the two regimes to be different. A possible solution

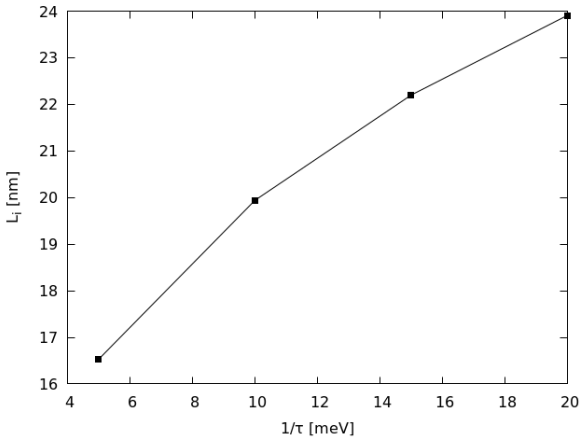

Figure 3.11: *In this figure, we report the behaviour of L_i vs $1/\tau$ extracted from the fit of theoretical DOS curves with experimental data*

to this *shape* issue, then, could rely in this difference between $T_c^{2\mathcal{D}}$ and $T_c^{0\mathcal{D}}$. We, therefore, carried out the DOS calculation replacing the formerly used constant $T_c^{2\mathcal{D}}$ with a more complex $T_c(\omega)$.

We expect that on long timescales, i.e. at small frequencies, the nature of fluctuations is mainly two-dimensional. On the other hand, at intermediate times, we hypothesise the diffusion to be anomalous, and to yeld a zero-dimensional like behaviour of fluctuating Cooper pairs. Therefore, we chose a ω dependence for the critical temperature such that at large energies $T_c(\omega) = T_c^{0\mathcal{D}}$, while in the region around $\omega = 0$ the two-dimensional critical temperature is restored. Among the possibilities, we used the inverse tangent function in the following form:

$$T_c(\omega) = T_c^{2\mathcal{D}} - \alpha(\frac{\pi}{2} + \beta \arctan(\gamma|\omega| - \delta)). \tag{3.39}$$

In figure 3.12 we report the chosen function for $T_c(\omega)$ for arbitrary parameters. For this figure, we used the critical temperature data from the thinner NbN sample (X_0) studied in [2].

Clearly modifying α, β, γ and δ the shape of the curve changes and it can be arranged to suitably fit the experimental data.

The result of the replacement of T_c with $T_c(\omega)$ is displaied in the two panels of figure 3.13, where we used exactly the same temperature and disorder strength of figure 3.10. After applying the modulation of the critical temperature with energy, the shape of our DOS curves immediately has a better agreement with the experimental data. Comparison with the curves obtained with constant critical temperatures shows that at intermediate energies, $T_c(\omega)$ gives the right result in the DOS, in satisfactory agreement with the data. Instead of a narrow dip around $\omega = 0$, as in fig.3.10, in this latter figures we find that the DOS shows a broadening in this region, as experimentally observed. Furthermore, at high frequencies, we restore the normal DOS, as indeed expected. This effect is clear, if we analyze the expression for $T_c(\omega)$. At higher energies $T_c(\omega) \sim T_c^{0\mathcal{D}} < T_c^{2\mathcal{D}}$. Therefore, at these energies, fluctuations feel more distant from the transition,

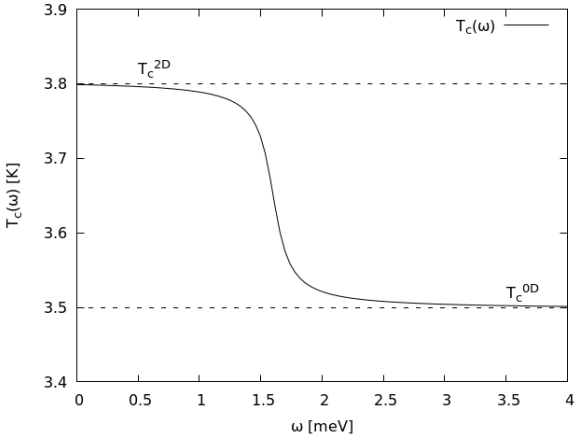

Figure 3.12: *Critical temperature $T_c(\omega)$ as resulting from eq.3.39. In this case we took critical temperature values of NbN sample X_0 of [2]*

and their effect decreases, leading to the reaching of the normal DOS value.

The figure in panel (a) shows the DOS calculated with $L_i = 16.5\ nm$, as in figure 3.10. In order to obtain the right agreement with experimental data (black crosses), we had to tune the parameter of eq.3.39. It is interesting to notice that in this figure we obtain a little overshooting at intermediate energies, as indeed is observed also in experiments. In panel (b), instead, we modifed the supergrains' size to a higher value $L_i = 35.3\ nm$ and again used the parameters in the $T_c(\omega)$ expression to obtain good agreement with experiments. We notice that in this latter case no overshooting is observed, and the DOS reaches a constant value at intermediate energies. The comparison of these two figures allows to understand that modifying $T_c(\omega)$ different DOS curves can be obtained.

Unfortunately, it is also straightforward that at small ω this description fails, and a cusp-like behaviour is still observed in the calculated curves. This characteristic seems to be typical of the dirty regime, as it is shown even in the standard diffusion limit, while in the clean case the behaviour at small energies is, at least qualitatively, in agreement with the experimental curves. This could point to a τ dependence on ω, suggesting that NbN thin films are in an intermediate disorder region. Unfortunately, at this stage, the switch from clean to dirty limit in our equations is quite cumbersome, and achieving a numerical solution to this issue is still complicated.

In conclusion, with this section we proved the effectiveness of the proposed anomalous diffusion law, $D\bar{q}^2 log(1 + \frac{q^2}{\bar{q}^2})$, in increasing the pseudogap, both in the clean and in the dirty limit of the two-dimensional superconductor. Furthermore, comparing the results of the two limits, we have been able to assess that among the two possibilities, certainly the dirty framework is the best to obtain the searched increase in pseudogap. Thus, we focused on this particular limit, obtaining good quantitative agreement (fig.3.10) with experimental data and establishing a relation between the dirtiness of the material and the supergrains' dimensions (fig.3.11). Encouraged by this success, we finally decided to explore a possible energy dependence of the critical temperature of the sample, passing from the two-dimensional to the zero-dimensional like regime. This last

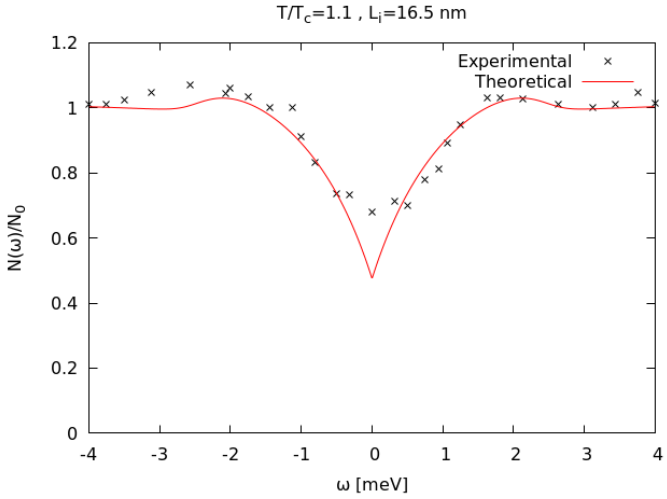

(a) *This figure was obtained employing the same parameters used to get figure 3.10:* $L_i = 16.5\ nm$, $1/\tau = 5\ meV$ *and* $T/T_c = 1.1$. *The adjustment of the variation of* T_c *gives the change in the shape of the curve. It is interesting to notice a little overshooting aroun* $\omega \sim 2\ meV$.

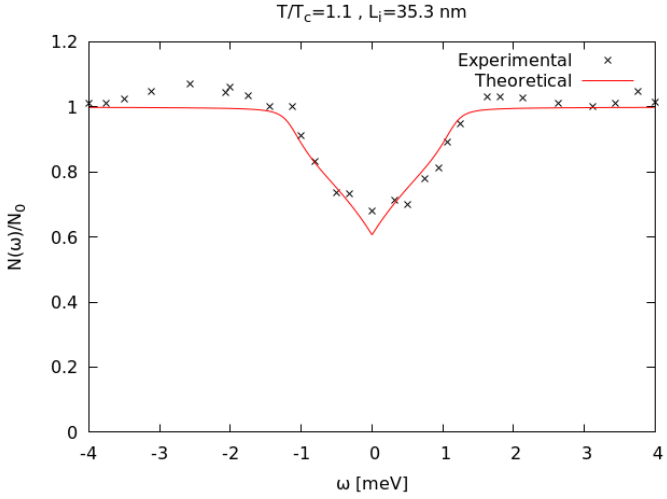

(b) *In this panel, we show a DOS curve calculated at the same temperature and impurity concentration previously used. Here, though, we changed the supergrains' size* L_i *and used different parameters in the* $T_c(\omega)$ *expression.*

Figure 3.13: *Comparison of the experimental data with a DOS curve obtained with* $T_c(\omega)$ *instead of constant critical temperature. A broadening in the region around* $\omega = 0$ *is observed, with respect to the result obtained in the same set up but with* $T_c = 3.8\ K$ *(fig.3.10)*

evaluation gave a satisfactory agreement with experimental data, as presented in figure 3.13, except for a small region around $\omega = 0$.

Chapter 4

Conclusions

As a conclusion to this thesis work, we would like to discuss the main results we were able to obtain, the limits of the model used, and the possible further developments, both theoretical and experimental.

As it is certainly clear to the carefull reader, our whole approach is purely phenomenological. Assuming the anomalous diffusion law, it has already been proven that paraconductivity anomalous behaviour highlighted in the paper by Carbillet et al. is explained in a satisfactory way. Nonetheless the physical mechanism behind this anomaly is, at this stage, still unknown.

With the calculation of the single electron density of states, we hoped to obtain at least a qualitative agreement with the conductance curves measured via Scanning Tunneling Spectroscopy on the samples and possibly grasp some other feature on the microscopical mechanism responsible of this anomalous diffusion.

In the two-dimensional particular case the paraconductivity has a quite universal behaviour, independent of the details of the material, such as its dirtiness. Thus, we had no initial suggestion on the right framework, whether the clean or the dirty one, to treat this system. Furthermore, NbN thin films present a mesoscopic type of disorder, giving rise to the supergrains, which could be generated by both standard microscopic disorder or another unknown mechanism. Therefore, both the frameworks could, in principle, give good results in the calculation of the pseudogap.

Applying quantum many body theory, we were able to obtain the DOS both in the clean and in the dirty case. Thus, in order to understand which of the two limits is better suited to explain this pseudogap enhancement in NbN films, we compared DOS curves obtained in the two cases. Studying these curves over a wide range of possible L_i values and of temperatures, we have been able to understand which of the frameworks was the most effective in showing the expected behaviour. This comparison proved that the dirty superconductor case is certainly the one in which the increase in the pseudogap is more evident.

This is the first achievement of this work: we discovered that microscopical disorder has a fundamental role in explaning pseudogap anomalies. This is not trivial as, for the reasons stated above, the nature of the mechanism that gives rise to anomalous diffusion was not predetermined.

We then studied in further detail the effect of anomalous fluctuations in the dirty superconductor. The investigation of the analytical expression for the

DOS with anomalous diffusion and our curves, obtained at different supergrains' size, disorder strengths and temperatures, lead to the understanding of the dependence of pseudogap on these quantities.

Since the starting point of this work was to find an explanation for the for the experimental tunnelling data on niobium nitride films, after identifying the dirty case as the best framework, we focused on comparing our theory with the experiments. We consequently investigated the possible fitting of our DOS curves with STS data, finding good quantitative agreement, concerning the increase in pseudogap with respect to the lower pseudogap regions highlighted in STS maps.

We therefore found that anomalous diffusion, together with the assumption of a disordered superconductor, can indeed explain the pseudogap enhancement measured in NbN samples. We also extracted some L_i values, all in satisfactory agreement with the results found in paraconductivity studies.

As a final result of this work, we were able to find the right parameter to modify the shape of our curves. Introducing an energy dependence of the critical temperature, we achieved a smoothening of the cusp-like dip at zero energy, reproducing the more rounded behaviour displayed by the experimental curves. This hypothesis was supported by the previous observation that the critical temperatures of the two regimes ($0\mathcal{D}$ and $2\mathcal{D}$) are different, hence we expect a *transition* with frequency. At low energies and long timescales, the system acts as a standard two-dimensional superconductor, while at higher energies and shorter lifetimes the anomalous diffusion sets in, yielding zero-dimensional like behaviour.

Our phenomenological description, then, can explain both the charge transport and the spectral properties of the electronic gas in two-dimensions, in NbN thin films. Nevertheless, as all these type of approaches, it will not reveal what is happening inside this superconductor at the microscopical level.

Therefore, the main future effort on this theme, should certainly be a deeper investigation on the microscopical mechanism ruling this anomalous diffusion. This study will probably be cumbersome, as many different issues complicate the derivation of the fundamental laws behind these phenomena. The interplay of different disorder types of different typical size is certainly one of them. It could, indeed, explain the intricate dependence of physical quantities on frequency, such as the $T_c(\omega)$ hypothesis we pursued in this thesis.

Another result that the investigation on the microscopical level could obtain is a different expression for the diffusion coefficient. We indeed expect this quantity to be modified by the same microscopical interaction that produces the supergrains structure. During all our calculations we used its standard value for the dirty superconductor, but we would not be surprised if another dependence would arise from the microscopical study. We started a preliminar analysis on the dependence of the diffusion coefficient on the supergrains' size L_i, but at this stage we do not have enough data to obtain a relevant hypothesis.

Another open issue is the cusp-like dip at zero energy in our DOS curves, which is absent in the experimental data that have a smooth rounded shape at zero bias. Many could be the different reasons for this discrepancy: for instance a distribution of L_i, $1/\tau$, and of the critical temperatures of the two-dimensional and zero-dimensional regimes over the sample. On the other hand, it could also be related to the intricate interplay of the different types of disorder. As a matter of fact, we observed that in the clean limit the dip has the correct

rounded shape, therefore we could also suggest that an intermediate disorder regime is present in this system.

Besides this theoretical investigation, further experimental studies are also necessary. It would be interesting to have experiments brought out on samples with different supergrains' dimension, with different impurity concentration or made of different compounds. The fabrication of other superconducting films with similar characteristics, indeed, would increase the understanding of their anomalous behaviours, and clarify many of the present open issues.

Appendices

Appendix A

Theoretical background

To account for fluctuations in disordered or low dimensional superconducting media both the phenomenological and the diagrammatic approach are efficient. Clearly, the first has a more *thermodynamic* character, studying the stability of the free energy functional to variations of the order parameter. The latter, instead, focuses on the microscopic nature of fluctuations, investigating the electron-electron interaction out of the mean field approximation.

In order to study fluctuations, we need to go beyond MFA. In G-L formalism, this is achieved considering a slowly varying complex order parameter, representing flucutating Cooper pairs, and adding a fluctuational term to the time-dependent G-L equation. In diagrammatic framework, we must give up the Hartree-Fock approximation, considering a fluctuation propagator, i.e. a simplified version of the four points Green function.

Even though both frameworks have much importance and highlight different aspects, this appendix has the target of being a brief help to the reader interested in the theoretical background of the physics presented in the main body of the thesis. For this reason, only some outstanding caluclations, relevant to the whole work, are reported here. Especially, we omit the phenomenological description at all, as the limits of validity of a microscopical approach are clearly wider, and furthermore this framework gives a better understanding of the physics of the system. We suggest the reading of [4] for an accurate review of the theory and of its applications.

The hamiltonian operator, in its BCS form, is:

$$\hat{H} = \sum_{\vec{k},\sigma} \xi_{\vec{k}} \hat{\psi}^{\dagger}_{\vec{k},\sigma} \hat{\psi}_{\vec{k},\sigma} - g \sum_{\vec{k},\vec{k}',\vec{q},\sigma,\sigma'} \hat{\psi}^{\dagger}_{\vec{k}+\vec{q},\sigma} \hat{\psi}^{\dagger}_{-\vec{k},-\sigma} \hat{\psi}_{-\vec{k}',-\sigma'} \hat{\psi}_{\vec{k}'+\vec{q},\sigma'} \tag{A.1}$$

.

Here, $\xi_{\vec{k}} = \varepsilon(\vec{k}) - \varepsilon_F$ and g is the electron-electron effective interaction constant, which is non-zero only in a narrow range of momenta near k_F.

A.1 The fluctuations' propagator

The mean field approximation performed in the standard BCS formulation consist of taking into account, for the calulation of the Green function's equation of

motion, only the one particle Green functions. If, instead, we consider the whole two-particles Green function $\mathcal{L}(k,k',q) =< T_\tau \hat{\psi}_{k+q,\sigma}\hat{\psi}_{-k,-\sigma}\hat{\psi}^\dagger_{k'+q,\sigma'}\hat{\psi}^\dagger_{-k',-\sigma'} >$, where T_τ is the τ-ordering operator and four-dimensional vector notation is understood, the situation complicates. In the following, we will call the fluctuation propagator $L(\vec{q},\Omega_k)$ the vertex part of the two particles Green function expansion. It is a chain of polarization bubbles in the particle-particle channel (as the arrows are oriented in the same direction), connected through phonon interactions, in the approximation in which this interaction is punctual. Its diagrammatic Dyson equation is expressed here below and it makes evident the dependence of it on the interaction constant g, represented by solid points, and on the polarization $\Pi(\vec{q},\Omega_k)$, expressed in random phase approximation (RPA) by single particle loops.

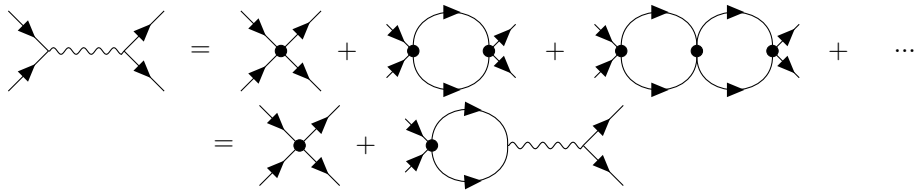

$$L(\vec{q},\Omega_k) = -g + g\Pi(\vec{q},\Omega_k)L(\vec{q},\Omega_k) \quad \Rightarrow L^{-1}(\vec{q},\Omega_k) = -\frac{1}{g} + \Pi(\vec{q},\Omega_k) \tag{A.2}$$

In order to evaluate the exact expression for $L(\vec{q},\Omega_k)$, we need to express the polarization in its analytic form:

$$\Pi(\vec{q},\Omega_k) = T\sum_{\omega_n}\int \frac{d^3k}{(2\pi)^3} G(\vec{k}+\vec{q},\omega_n+\Omega_k)G(-\vec{k},-\omega_n). \tag{A.3}$$

Since the single-electron Green functions that appear in eq.A.3 are the ones of the normal metal, we can rewrite the equation replacing $G(\vec{k},\omega_n) = \frac{1}{\imath\omega_n - \xi_k}$:

$$\Pi(\vec{q},\Omega) = T\sum_{\omega_n}\int \frac{d^3k}{(2\pi)^3}\frac{1}{\imath(\omega_n+\Omega)-\xi_{k+q}}\frac{1}{-\imath\omega_n-\xi_{-k}} \tag{A.4}$$

In a small shell in the vicinity of the Fermi surface, the following approximation for the quasi-particle energy is reasonable:

$$\xi_{k+q} \approx \xi_k + \nabla_k\xi_k\cdot\vec{q} = \xi_k + \vec{v}_k\cdot\vec{q} \tag{A.5}$$

the integral thus can be solved separating the angular part $\int \frac{d\Omega}{4\pi^2} =<>_{F.S.}$ and replacing the residual integration over wave-vectors $\vec{k}$ with an integral over the energies ξ, being N the density of states:

$$\begin{aligned}
\Pi(\vec{q},\Omega) &= T\sum_{\omega_n} N\Big\langle -\int d\xi \frac{1}{\imath\omega+\xi}\frac{1}{\imath(\omega+\Omega)-\xi-\vec{v}_k\cdot\vec{q}}\Big\rangle_{F.S.} \\
&= T\sum_{\omega_n} N2\pi\theta(-\omega(\omega+\Omega))\Big\langle\frac{1}{(2\omega+\Omega)(1+\imath\frac{\vec{v}_k\cdot\vec{q}}{2\omega+\Omega})}\Big\rangle_{F.S.} \\
&\approx T\sum_{\omega_n} N2\pi\theta(-\omega(\omega+\Omega))\frac{1}{2\omega+\Omega}\Big(1-\frac{\big\langle(\vec{v}_k\cdot\vec{q})^2\big\rangle_{F.S}}{(2\omega+\Omega)^2}\Big).
\end{aligned} \tag{A.6}$$

In the first step we use analytic continuation of the function in ξ in order to use the residue theorem and solve the integral in the lower half complex plane (the upper half would give the same result, clearly). To obtain the result in the third row, we take advantage of the fact that in the narrow region in the vicinity of the critical temperature we are considering, $\vec{v}_k \cdot \vec{q} \ll T \sim \omega$ always, thus the expansion of the denominator is possible in the way we chose, obtaining the final expression.

Exlpoiting the sum over the fermionic Matsubara frequencies $\omega_n = 2\pi T(n + 1/2)$, the sequent result is found for the polarization:

$$\Pi(\vec{q},\Omega) = N\Big[\sum_{n\geq 0} \frac{1}{n+\frac{1}{2}+\frac{|\Omega|}{4\pi T}} - \frac{<(\vec{v}_k\cdot\vec{q})^2>_{F.S.}}{(4\pi T)^2}\sum_{n\geq 0}\frac{1}{(n+\frac{1}{2}+\frac{|\Omega|}{4\pi T})^2}\Big] \quad \text{(A.7)}$$

These sums can be evaluated by the calculation of the digamma function $\psi(x)$ defined as the logarithmic derivative of the Euler gamma function: $\psi^{(n)}(x) = \frac{d^n}{dx^n} log(\Gamma(x))$. The first sum, which is indeed logarithmically divergent at $n \to \infty$, is known as the *Cooper logarithm* and its divergence is cut-off by the Debye energy. The final expression for the polarization is thus:

$$\Pi(\vec{q},\Omega) = N\Big[\psi(\frac{1}{2}+\frac{|\Omega|}{4\pi T}+\frac{\omega_D}{2\pi T})-\psi(\frac{1}{2}+\frac{|\Omega|}{4\pi T})+\frac{<(\vec{v}_k\cdot\vec{q})^2>_{F.S.}}{2(4\pi T)^2}\psi''(\frac{1}{2}+\frac{|\Omega|}{4\pi T})\Big] \quad \text{(A.8)}$$

From BCS theory's determination of critical temperature, we can get the value of the interaction constant g:

$$T_c = \frac{2\gamma}{\pi}\omega_D e^{-\frac{1}{gN}} \quad \to \quad -\frac{1}{g} = N log(\frac{\pi}{2\gamma\omega_D}T_c) \quad \text{(A.9)}$$

Being $\gamma = e^C$, where C is the Euler-Mascheroni constant ($\psi(\frac{1}{2}) = -2log2 - C$). Using this relation, and recalling that $\psi(\frac{1}{2}+z) \approx log(z)$, the expression for the fluctuations' propagator in eq.A.2 is found to be:

$$L(\vec{q},\Omega) = -\frac{1}{N}\frac{1}{\epsilon + \psi(\frac{1}{2}+\frac{|\Omega|}{4\pi T}) - \psi(\frac{1}{2}) - \frac{<(\vec{v}\cdot\vec{q})^2>_{F.S.}}{2(4\pi T)^2}\psi''(\frac{1}{2}+\frac{|\Omega|}{4\pi T})}. \quad \text{(A.10)}$$

Acknowledgments

I would like to acknowledge, for supporting me in these months, many people. First of all, Professor Marco Grilli for accepting me as a thesis student even if I came from another University and for the time spent discussing unclear features and results as they came by during this work. Together with him, I must thank Professor Sergio Caprara, who also took part to these proficuous talks, and Professor Luca Molinari, who, although we've been in different cities during much time of the thesis, always looked at this work with sincere interest and firstly opened my eyes to the intriguing world of quantum many body theory.

Thank you to my family and friends, for being by my side through all these years. This path, without all of you, would have been much harder to travel. If I am here today, discussing this thesis, is certainly also because of your support either in the though or in the easy times.

To my faculty friends, with whom I spent a huge amount of time in these years. We shared all of this together, growing up and learning together. You made this period of my life unforgettable: Steve, the first of us to get his degree (I would have bet on this), and his barbecues at the lake, Reggia, with his ganja obsession, who's one of the most genial people I've ever met, Longo and his *scialla*, *paleeese* and a lot of funny vocabulary, Arrighi, always searching for answers to his not-so-trivial questions, Mario, his saturday morning calls to ask whatsoever, but also the beers together at his place, the nights out and Parma's Christmas lunch, Luigi, who unexpectedly came back from Ciociaria, determined to finish the studies and Vitto & Tom, who at this point are always mentioned together, with their University career made of sprints and of periods of total absence, will they finally get a thesis? I wish to all of you the best and I ask you, us, to do our best to keep in touch, even now that University is over.

A special thanks goes to Carlo and Roberto, whose friendly wisdom, guided me in though decisions.

I would like to thank my rugby team, Stella Rossa Rugby Milano, a deep feeling binds all of us together, which, you know, goes well beyond the simple being sportmates. It's being a team, that, for the ones who can understand me, has a total different meaning.

Last, but definitely not least, to my love, Chicca. You have been there since the very start, pushing me towards the final step, through good and bad times. You own this, let's hope it is indeed, success as much as I do.

To all of you, my very special thanks, from the bottom of my heart.

Bibliography

[1] E. Abrahams, M. Redi and J. Woo *Phys. Rev. B* **1** 208-213 (1970)

[2] C. Carbillet, S. Caprara, M. Grilli et al. *Phys. Rev. B* **93** 144509 (2016)

[3] C. Di Castro, R. Raimondi, C. Castellani and A.A. Varlamov *Phys. Rev. B* **42** 10211 (1990)

[4] A. Larkin and A. Varlamov *Theory of fluctuations in superconductors* Oxford University Press (2005)

[5] H. Kamerling Onnes *Leiden Communications* **122b** 124 (1911)

[6] F. London and H.London *Proceedings of the Royal Society* **A149** 71 (1935)

[7] W. Meissner and R. Ochsenfeld *Naturwissenschaften* **21** 787 (1933)

[8] V.L. Ginzburg and L.D. Landau *Zh. Eksp. Teor. Fiz.* **20** 1064 (1950)

[9] L.D. Landau *Zh. Eksp. Teor. Fiz.* **7** 19 (1937)

[10] A.A. Abrikosov *Zh. Eksp. Teor. Fiz.* **32** 1442 (1957)

[11] L.V. Shubnikov, V.I. Khotkevich et al. *Zh. Eksp. Teor. Fiz.* **7** 221 (1937)

[12] H. Froelich *Phys. Rev.* **79** 845 (1950)

[13] L.N. Cooper *Phys. Rev.* **104** 1189 (1956)

[14] J. Bardeen, L.N. Cooper and J.R. Schriffer *Phys. Rev.* **106** 162 (1957)

[15] L.P. Gor'kov *Zh. Eksp. Teor. Fiz.* **34** 735 (1958)

[16] L.P. Gor'kov *Zh. Eksp. Teor. Fiz.* **37** 1407 (1959)

[17] L.G. Aslamazov and A.I. Larkin *Soviet Solid State Physics* **10** 875 (1968)

[18] R.E. Glover *Phys. Rev. L.* **A25** 542 (1967)

[19] V. Ginzburg *Soviet Solid State Physics* **2** 61 (1960)

[20] K. Bouadim et al. *Nature Physics* **7** 884 (2011)

[21] M. Strongin et al. *Phys. Rev. Lett* **20** 922 (1968)

[22] S.P. Farrant and C.E. Gough *Phys. Rev. Lett.* **34** 943 (1975)

[23] B. Sacépé et al. *Nature Communications* **1** 140 (2010)

[24] R.W. Cohen, B. Abeles and C.R. Fuselier *Phys. Rev. Lett.* **23** 377 (1969)

[25] B. Sacépé et al. *Phys. Rev. Lett.* **101** 157006 (2008)

[26] A. Kamlapure et al. *Sci. Rep.* **3** 2979 (2013)

[27] B.L. Altshuler, A.G. Aronov and P.A. Lee *Phys. Rev. Lett.* **44** 1288 (1980)

[28] K. Maki *Prog. Theor. Phys.* **40** 193 (1968)

[29] R.S. Thompson *Phys. Rev. B* **1** 327 (1970)

[30] B.I. Belevstsev and Yu F. Komnik *Sov. J. of Low Temp. Phys.* **9** 3 (1983)

[31] M.P.A. Fisher et al. *Phys. Rev. B* **40** 546 (1989)

[32] N.F. Mott *Rev. Mod. Phys.* **40** 677 (1968)

[33] P.W. Anderson *Phys. Rev.* **109** 1492 (1958)

[34] N. Marković et al. *Phys. Rev. B* **60** 4320 (1999)

[35] M.P.A. Fisher, G. Grinstein and S.M. Girvin *Phys. Rev. Lett.* **64** 587 (1990)

[36] M.P.A. Fisher *Phys. Rev. Lett.* **65** 923 (1990)

[37] M. Wallin et al. *Phys. Rev. B* **49** 12115 (1994)

[38] T. Wang et al. *Phys. Rev. B* **47** 11619 (1993)

[39] T. Wang et al. *Phys. Rev. B* **43** 8623 (1991)

[40] S. Tanda, S. Ohzeki and T. Nakayama *Phys. Rev. Lett.* **69** 530 (1992)

[41] J.M. Valles, R.C. Dynes and J.P. Garno *Phys. Rev. B* **50** 6680 (1989)

[42] J.M. Valles, R.C. Dynes and J.P. Garno *Phys. Rev. Lett.* **69** 3567 (1992)

[43] M.A. Paalanen, A.F. Hebard and R.R. Ruel*Phys. Rev. Lett.* **69** 1604 (1992)

[44] A. Yazdani and A. Kapitulnik *Phys. Rev. Lett.* **74** 3037 (1995)

[45] A. Shalnikov *Nature* **142** 74 (1938)

[46] B. Abeles, R.W. Cohen and G.W. Cullen *Phys. Rev. Lett.* **17** 632 (1966)

[47] E.A. Lynton, B. Serin and M. Zucker *J. Phys. Chem. Solids* **3** 165 (1957)

[48] A.M. Finkel'stein *Pis'ma ZhETF* **45** 37 (1987) [*JETP Lett* **45** 46 (1987)]

[49] M. Strongin et al. *Phys. Rev. B* **1** 1078 (1970)

[50] A.M. Finkel'stein *Physica B* **197** 636 (1994)

[51] H. Takagi an Y. Kuroda *Solid State Comm.* **41** 643 (1982)

[52] S. Mackawa and H. Fukuyama *J. Phys. Soc. Jpn* **51** 1380 (1982)

[53] P.W. Anderson *J. Phys. Chem. of Solids* **11** 26 (1959)

[54] N. Trivedi et al. *J. Phys.: Conf. Ser.* **376** 012001 (2012)

[55] L.J. Geerligs et al. *Phys. Rev. Lett.* **63** 326 (1989)

[56] M.A. Steiner, N.P. Breznay and A. Kapitulnik *Phys. Rev. B* **77** 212501 (2008)

[57] D.B. Haviland, Y. Liu and A.M. Goldman *Phys. Rev. Lett.* **62** 2180 (1989)

[58] A. Semenov et al. *Phys. Rev. B* **80** 054510 (2009)

[59] J. Wen-He et al. *New J. Phys.* **15** 113002 (2013)

[60] A.P. Levanyuk *Zh. Eksp. Teor. Fiz.* **30** 810 (1959)

[61] J. Kirtley, Y. Imry and P.K. Hansma *J. Low Temp. Phys.* **17** 247 (1974)

[62] S. Wolf and W.H. Lowrey *Phys. Rev. Lett.* **39** 1038 (1977)